



**INTELLECTUAL
PROPERTY INDIA**

PATENTS | DESIGNS | TRADE MARKS
GEOGRAPHICAL INDICATIONS



सत्यमेव जयते

क्रमांक : 044126373
SL No :



भारत सरकार
GOVERNMENT OF INDIA

पेटेंट कार्यालय
THE PATENT OFFICE

पेटेंट प्रमाणपत्र
PATENT CERTIFICATE
(Rule 74 Of The Patents Rules)

पेटेंट सं. / Patent No. : 356814
आवेदन सं. / Application No. : 201841049836
फाइल करने की तारीख / Date of Filing : 29/12/2018
पेटेंटी / Patentee : INDIAN INSTITUTE OF TECHNOLOGY MADRAS (IIT Madras)

प्रमाणित किया जाता है कि पेटेंटी को उपरोक्त आवेदन में यथाप्रकटित A PROCESS FOR LOW TEMPERATURE, LOW PRESSURE SYNTHESIS OF GAS HYDRATES नामक आविष्कार के लिए, पेटेंट अधिनियम, १९७० के उपबंधों के अनुसार आज तारीख 29th day of December 2018 से बीस वर्ष की अवधि के लिए पेटेंट अनुदत्त किया गया है।

It is hereby certified that a patent has been granted to the patentee for an invention entitled A PROCESS FOR LOW TEMPERATURE, LOW PRESSURE SYNTHESIS OF GAS HYDRATES as disclosed in the above mentioned application for the term of 20 years from the 29th day of December 2018 in accordance with the provisions of the Patents Act, 1970.



अनुदान की तारीख : 27/01/2021
Date of Grant :

पेटेंट नियंत्रक
Controller of Patent

टिप्पणी - इस पेटेंट के नवीकरण के लिए फीस, यदि इसे बनाए रखा जाना है, 29th day of December 2020 को और उसके पश्चात प्रत्येक वर्ष में उसी दिन देय होगी।

Note. - The fees for renewal of this patent, if it is to be maintained will fall / has fallen due on 29th day of December 2020 and on the same day in every year thereafter.

FORM 2
THE PATENTS ACT, 1970
(39 OF 1970)
&
The Patents Rules, 2003
COMPLETE SPECIFICATION
(Refer section 10 and rule 13)

TITLE OF THE INVENTION:

A PROCESS FOR LOW TEMPERATURE, LOW PRESSURE SYNTHESIS OF CLATHRATE HYDRATES

2. APPLICANT:

(A) NAME: **INDIAN INSTITUTE OF TECHNOLOGY MADRAS (IIT Madras)**

(B) NATIONALITY: Indian

(C) ADDRESS: **INDIAN INSTITUTE OF TECHNOLOGY MADRAS**

IIT P.O

Chennai - 600 036

3. Preamble to the Description

COMPLETE SPECIFICATION

The following specification particularly describes the invention and the manner in which is to be performed.

COMPLETE SPECIFICATION

TITLE OF THE INVENTION

5 **A PROCESS FOR LOW TEMPERATURE, LOW PRESSURE SYNTHESIS OF CLATHRATE HYDRATES**

FIELD OF THE INVENTION

10 The present invention relates to the formation of gas hydrates in an environment analogous to interstellar medium (ISM). More specifically the present invention relates to formation of methane, carbon dioxide, acetone and tetrahydrofuran hydrates in interstellar environment.

BACKGROUND OF THE INVENTION

15 Clathrate hydrates (CHs) are crystalline inclusion compounds in which different guest molecules are encased in H-bonded water-cages [Sloan Jr ED, *Nature*, **2003**, 426:353-363]. These trapped molecules are generally small such as CH₄, CO₂, N₂, H₂, etc. Among several such known CHs, those of CH₄ and CO₂ have drawn close attention of the scientific community due to their use as potential future source of energy [Sloan Jr ED, *Nature*, **2003**, 426:353-363, Walsh MR, 20 Koh CA, Sloan ED, Sum AK, & Wu DT, *Science*, **2009**, 326(5956):1095-1098] and in CO₂ sequestration [Park Y, et al., *Proc. Natl. Acad. Sci. U.S.A.*, **2006**, 103(34):12690-12694], respectively. Natural methane and carbon dioxide hydrates are found in permafrost and marine sediments on the outer continental shelves [Boswell R, *Science*, **2009**, 325(5943):957-958] at ambient temperatures (<300 K) and moderately high pressures (6 atm) [Sloan Jr ED, *Nature*, 25 **2003**, 426:353-363]. They could also exist in many solar system bodies such as Martian permafrost [Chastain BK & Chevrier V, *Planet. Space Sci.*, **2007**, 55(10):1246-1256, Swindle TD, Thomas C, Mousis O, Lunine JI, & Picaud S, *Icarus*, **2009**, 203(1):66-70, Thomas C, Mousis O, Picaud S, & Ballenegger V, *Planet. Space Sci.*, **2009**, 57(1):42-47], on the surface of Titan [Tobie G, Lunine JI, & Sotin C, *Nature*, **2006**, 440:61-64] and other icy satellites due to the prevalent 30 thermodynamic (high P, low T) conditions [Mousis O, Lunine JI, Picaud S, & Cordier D, *Faraday Discuss.*, **2010**, 147(0):509-525]. The stabilizing conditions (generally high pressures) of methane hydrate suggest that it is non-existent in ultrahigh vacuum (UHV). Near zero

diffusion prevents molecular rearrangements at cryogenic conditions, making the formation of cage structures impossible for water at interstellar temperatures. Therefore, it is not surprising that there is no report on its existence in conditions of relevance to space. Using thermodynamic data of methane hydrate available in the literature, its stability was extrapolated to low T, P region as shown (Fig. 4), which suggests stability up to 2×10^{-6} mbar at 30 K. This temperature and pressure range is very close to nebular pressures which could reach as high as 10^{-3} mbar and the temperature range can vary from 4 to 100 K [Mousis O, Lunine JI, Picaud S, & Cordier D, *Faraday Discuss.*, **2010**, *147(0)*:509-525]. Equilibrium condensation curve of methane hydrate in protostellar nebula (PSN) also suggests its stability $\sim 1 \times 10^{-8}$ mbar at 45 K [Luspay-Kuti A, et al., *Sci. Adv.*, **2016**, *2(4)*:e1501781].

Experimentally, in-situ formation of CHs in UHV and cryogenic interstellar conditions has not been explored. However, it was proposed that at low-pressure, CH may be grown epitaxially on other preformed CHs or by annealing the condensed gas-water mixture [Mao WL, et al., *Science*, **2002**, *297(5590)*:2247-2249]. CH of CO₂ was obtained in a vacuum of 10^{-6} torr, but at 120 K [Blake D, Allamandola L, Sandford S, Hudgins D, & Freund F, *Science*, **1991**, *254(5031)*:548-551]. The present invention have adopted the annealing method to obtain CHs. In experiments conducted in the temperature window of 10-160 K and at 10^{-10} mbar pressure, observed CH₄ and CO₂ hydrates at temperatures near 30 and 10 K, respectively. Molecular mobility and structural rearrangement observed in these experiments at cryogenic conditions suggest unusual processes in water. The anomalous eruption of CH₄, CO₂ or other volatile gases in cold interstellar clouds or in comets could possibly be explained by the existence of such hydrates in gas forming regions of the interstellar space [Luspay-Kuti A, et al., *Sci. Adv.*, **2016**, *2(4)*:e1501781, Blake D, Allamandola L, Sandford S, Hudgins D, & Freund F, *Science*, **1991**, *254(5031)*:548-551]. Irradiation or annealing leads to the chemical evolution of ice in ISM, forming new species [Allamandola LJ, Bernstein MP, Sandford SA, & Walker RL, *Space Sci. Rev.*, **1999**, *90(1-2)*:219-232]. CHs could be one such new chemical system in the ISM, which may be subjected to additional processing.

Formation of clathrate hydrate (CH) requires high-pressures and moderate temperatures which enable their existence in marine sediments and permafrost region of earth. The presence of CHs in interstellar medium (ISM) is still in question due to the extreme high vacuum and ultra-cold conditions present there. Here, the present invention conclusively identified methane,

carbon dioxide, acetone and tetrahydrofuran hydrates in conditions analogous to ISM. The present invention found that the molecular mobility and interactions play crucial roles in the formation of CHs, even though there is no external pressure to force cage formation. Various chemical processes on these hydrates in ISM may lead to relevant prebiotic molecules.

5

SUMMARY OF THE INVENTION

The invention describes a process for synthesizing clathrate hydrates in extreme low-pressure environments analogous to interstellar medium (ISM). More specifically the present invention relates to formation of methane, carbon dioxide, acetone and tetrahydrofuran hydrates in extreme low-pressure environments. These hydrates in ISM, subjected to various chemical processes that act as sources for relevant prebiotic molecules.

The process for synthesizing clathrate hydrates in ultrahigh vacuum at low pressure of 10^{10} mbar and at temperatures up to 10 K, wherein the said process comprises, condensing the vapours separately or together; gradually annealing the condensed mixture to temperatures below the desorption temperature of the substance in the vacuum and waiting for the time in the range of 0-48 hours for the formation of clathrate hydrates.

In one embodiment, the present invention relates to the formation of methane and carbon dioxide hydrates in an ultrahigh vacuum chamber that analogous to interstellar medium (ISM). Thermal treatment of solid methane and carbon dioxide-water mixture in ultrahigh vacuum of the order of 10^{-10} mbar for extended periods, leads to the formation of clathrate hydrates (CHs) at 30 K and 10 K, respectively. High molecular mobility and H-bonding play important roles in the entrapment of gases in the in-situ formed 5^{12} CH cages. It implies that CHs can exist in extreme low-pressure environments present in the ISM.

In other embodiment, the present invention relates to the formation of acetone hydrates in an ultrahigh vacuum chamber (UHV) that analogous to interstellar medium (ISM). Acetone hydrate was prepared by annealing a co-deposited ~ 300 MLs acetone:H₂O (1:1) film to 135 K, wherein acetone hydrate transforms into cubic crystalline ice I_c upon in-situ dissociation at 130-135 K over 3 hours.

In another embodiment, the present invention illustrates the formation of tetrahydrofuran (THF) hydrate in an ultrahigh vacuum chamber (UHV) by co-depositing a 1:5 mixture of THF and water from their vapour phase to a precooled Ru(0001) substrate at 10 K inside a UHV

chamber. Annealing the mixture to 130 K and keeping it for 6 hours led to the formation of THF hydrate at 10^{-10} mbar.

BRIEF DESCRIPTION OF THE DRAWINGS

5 **Figure 1** shows CH₄ hydrate formation as studied by RAIR spectroscopy and quantum chemical calculations.

Figure 2 shows CO₂ hydrate formation as studied by RAIR spectroscopy and quantum mechanical calculations.

Figure 3 shows TPD mass spectra of 300 MLs of co-deposited ice systems at different ratio.

Figure 4 shows equilibrium curve for CH₄ clathrate hydrate.

10 **Figure 5** shows time dependent RAIR spectra of 150 MLs of solid CH₄ in the C-H antisymmetric stretching region at 25 K.

Figure 6 shows temperature dependent RAIR spectra of 300 MLs of CO₂@H₂O (1:5 ratio) in the C=O antisymmetric stretching region.

Figure 7 shows full scale RAIR spectrum of 300 MLs of CO₂+H₂O (1:5 ratio) at 10 K.

15 **Figure 8** shows temperature dependent RAIR spectra of 300 MLs of CO₂+H₂O (1:5 ratio) in the ¹³C=O antisymmetric region.

Figure 9 shows TPD mass spectra of 150 MLs of solid CH₄ and CH₄+H₂O co-deposited ice systems at different ratios (heating rate of 30 K.min⁻¹).

20 **Figure 10** RAIR spectra of 300 MLs of acetone: H₂O (1:1) at 135 K in the O-H and C=O stretching regions. The mixture was co-deposited on Ru(0001) substrate at 10 K, and annealed at a rate of 2 K.min⁻¹ to 135 K. The C=O stretching band was deconvoluted to show the concentration of acetone trapped in the hydrate cage and ASW pores. Inset focuses on the change in C=O stretching band upon dissociation of acetone hydrate over time. The O-H band changed after crystallization and different features were resolved upon deconvolution.

25 **Figure 11** Time-dependent RHEED images of 300 MLs of acetone:H₂O (1:1) at 120, 130, and 135 K. Here, a co-deposition was done on Ni(111) substrate at 20 K by following a similar method as in a RAIRS study. After deposition, the mixtures were annealed at 2 K.min⁻¹ to reach the required temperatures. RHEED images were collected at 135 K for (a) 0 h and (b) 5 h; 130 K for (c) 0 h and (d) 12 h; 120 K for (e) 0 h and (f) 24 h.

30 **Figure 12** TPD-MS spectra of 300 MLs of acetone:H₂O (1:1). The ramping rate was 30 K.min⁻¹. Here, the intensities of CH₃CO⁺ (m/z = 43) and H₂O⁺ (m/z = 18) are plotted. (a) Desorption trace

of acetone ($m/z = 43$) shows a sharp peak at 134 K which is attributed to the untrapped acetone desorption. The shoulder labelled \$ is due to acetone hydrate desorption. Peak labelled * is attributed to acetone desorption due to pre-melting of ice upon annealing and that labelled # is due to desorption of acetone along with the processes in ice. (b) Desorption trace of water ($m/z = 18$) shows a side band which is due to the amorphous to crystalline ice transition. It coincides with the shoulder labelled \$. Peak at 155 K is due to the complete desorption of ice.

Figure 13 Time-dependent RAIR spectra of 300 MLs of acetone: HDO (5% D₂O in H₂O) at 135 K in the (a) O-H stretching region, and (b) O-D stretching region. The mixture was co-deposited on Ru(0001) substrate at 10 K, and annealed at a rate of 2 K min⁻¹ to 135 K. The vertical lines at a fixed wave number are used to measure the absorbance changes with time, which was further utilized for calculation of crystallization fraction.

Figure 14 Crystallization fraction of 300 MLs of acetone:HDO (5% D₂O in H₂O) obtained from isothermal RAIRS measurements at 130, 132, 135, and 137 K. The extent of crystallization were estimated from, (a) the 3307 cm⁻¹ peak in the O-H stretching region, and (b) the 2427 cm⁻¹ peak in the decoupled O-D stretching region.

Figure 15 Plot of $\ln(-\ln[1-x(t)])$ vs. $\ln(t)$ at different temperatures of 130, 132, 135, and 137 K. These data points are obtained from the analysis of (a) the O-H, and (b) the O-D stretching regions and fitted using Avrami equation (eqn. 3). Plot of $\ln k(T)$ vs. inverse temperature ($1/T$), obtained from the analysis of (c) the O-H, and (d) the O-D stretching regions, respectively. The data points were fitted to obtain a straight line. Activation energy (E_a) can be calculated from the slope of the straight line.

Figure 16 Isothermal time-dependent RAIR spectra of 300 MLs of a THF:H₂O (1:5) mixture (a) in the asymmetric C-O stretching region, and (b) in the O-H stretching region, at 130 K. Prior to data collection, the mixture was co-deposited on Ru(0001) substrate at 10 K, and annealed at a rate of 2 K min⁻¹ to 130 K. In (b), spectrum labeled 6 h was deconvoluted to show its components and the spectrum of ASW was multiplied by 1.5 to match the intensity with the former.

Figure 17 Time-dependent RAIR spectra of 300 MLs of a THF@H₂O mixture (1:1) in (a) asymmetric C-O stretching region, and (b) in O-H stretching region, which was sequentially deposited at 10 K on Ru(0001) substrate. This mixture was annealed at a rate of 2 K min⁻¹ to 130

K. In (b), spectrum labeled 6 h was deconvoluted to show its components and the spectrum of ASW was multiplied by 1.5 to match the intensity with the former.

Figure 18 Temperature-dependent RAIR spectra of 300 MLs of a THF@H₂O mixture (1:1) in (a) asymmetric C-O stretching region, and (b) in O-H stretching region, which was sequentially deposited at 10 K on Ru(0001) substrate. The sequential deposition was carried by condensing 150 MLs of H₂O film over the same coverage of THF film, thus making it a (1:1) mixture. This mixture was annealed at 2 K min⁻¹ heating rate and the spectra were collected.

Figure 19 Time-dependent RAIR spectra of 300 MLs of a THF:H₂O mixture (1:5) at (a) 120 K, and (b) at 125 K, in the asymmetric C-O stretching region, the mixture was co-deposited at 10 K on the Ru(0001) substrate. This mixture was annealed at 2 K min⁻¹ to the respective temperatures. Variation of the IR peak intensities of 1053 and 1074 cm⁻¹, plotted as contour plot as a function of time at (c) 120 K, and (d) 125 K. Intensity values are on the right.

Figure 20 (a) Plot of $\ln(-\ln[1-y(T)])$ vs. $\ln(t)$ at different temperatures of 130, 125, and 120 K. The data points were fitted using Avrami equation (eqn. 2). These data correspond to a straight line. (b) Plot of $\ln k(T)$ vs. inverse temperature ($1/T$). The data points were fitted to obtain the straight line. Activation energy (E_a) can be calculated from the slope of the straight line.

Figure 21 DFT-optimized structures of THF trapped within different CH cages, such as, (a) 5¹²6⁴ cage, (b) 5¹² cage, and (c) 5¹²6² cage. Here, water cage and the guest molecule (THF) are shown. H atoms of THF molecules in all the structures are omitted for clarity. Color code used: cyan, C; red, O; gray, H.

Referring to the drawings, the embodiments of the present invention are further described. The figures are not necessarily drawn to scale, and in some instances the drawings have been exaggerated or simplified for illustrative purposes only. One of ordinary skill in the art may appreciate the many possible applications and variations of the present invention based on the following examples of possible embodiments of the present invention.

DETAILED DESCRIPTION OF THE INVENTION

As required, detailed embodiments of the present invention are disclosed herein; however, it is to be understood that the disclosed embodiments are merely exemplary of the

invention that may be embodied in various forms. The figures are not necessarily to scale; some features may be exaggerated to show details of particular components.

The following description describes the process for synthesizing gas hydrates in extreme low-pressure environments. Particularly, the invention describes a process for the formation of methane, carbon dioxide, acetone and tetrahydrofuran hydrates in an environment like UHV that
5 analogous to ISM.

Example 1

Experimental set-up and sample preparation

Materials and Methods

10 Experiments were conducted in an ultrahigh vacuum (UHV) instrument (base pressure $\sim 10^{-10}$ mbar). This order of vacuum is an essential condition for the interstellar medium (ISM). Vacuum was maintained by oil-free Turbo molecular pumps (TMP) backed by diaphragm pumps. A thin film of ice was grown on top of a Ru(0001) single crystal that was mounted on a copper holder, which in turn, was attached at the tip of a closed cycle helium cryostat (Sumitomo
15 Cryogenics). The substrate temperature could be controlled from 8 to 1000 K. For the present study, the temperature was measured by a thermocouple sensor attached to the substrate. Repeated heating to 300 K prior to vapor deposition ensured surface cleanliness, adequate for the present experiments. Temperature ramping was controlled and monitored by a temperature controller (Lakeshore 336).

20 For the formation of methane hydrate, $\sim 99.99\%$ pure methane gas, purchased from Rana Industrial Gases & Products, India was used. The gas line was connected to the experimental chamber through a high precision all-metal leak valve, using which the flow rate or deposition pressure of different gases was controlled. Out of the two sample inlet lines, one was used exclusively for methane or carbon dioxide while the other line was used exclusively for water
25 vapor deposition. Here, Millipore water (H_2O of 18.2 M Ω resistivity), taken in a test tube, connected to the sample line through a glass-to-metal seal was used for the experiment. The Millipore water was further purified through several freeze-pump-thaw cycles before introduction into the UHV chamber. During the exposure of different samples into the UHV chamber, mass spectra were recorded with a residual gas analyzer (RGA) attached near to the
30 sample inlet line. Recorded mass spectra were used as an indication of the purity of the samples as well as to measure the ratio of the mixtures. The ratio of the mixed ice was achieved by the

proper adjustment of flow or inlet pressure of the sample gas. The substrate was kept at a perpendicular position for the uniform growth of ice. Here, most of the experiments were performed using 300 MLs coverage of the mixed ice. The deposition of molecular solids was controlled through leak valves, and monolayer (ML) coverage was calculated assuming that
5 1.33×10^{-6} mbar.s = 1 ML which was estimated to contain $\sim 1.1 \times 10^{15}$ molecules.cm⁻². The inlet pressure during the sample deposition was decided based on the coverage desired at the time of the experiment.

For the deposition of 300 MLs of (1:1) mixed methane and ice, the chamber was backfilled at a total pressure of $\sim 5 \times 10^{-7}$ mbar (where, methane pressure was 2.5×10^{-7} mbar, and water
10 pressure was 2.5×10^{-7} mbar) and the mixture was exposed to the surface for 10 minutes. This mixed ice was slowly (heating rate = 2 K.min⁻¹) heated to 30 K, near the desorption temperature of methane. At this temperature, most of the methane sublimed, which was observed in the mass spectra recorded by the residual gas analyzer. After that, the remaining mixed ice was maintained at 30 K for over 25 hours. The ice sample was constantly monitored by IR spectroscopy. In other
15 words, time-dependent reflection absorption infrared spectra (RAIRS) were recorded over a period of 25 hours. Similar time-dependent RAIR study was carried out at 10 and 20 K also. IR exposure over extended periods did not have an effect on CH formation as revealed by studies at lower temperatures.

For the CO₂ hydrate formation, 300 MLs of mixed ice was made by the co-deposition of a
20 mixture of CO₂:H₂O on the substrate at 10 K. Different ratios (1:5, 1:10, and 1:90) of CO₂:H₂O were used. For each of the ratios, the total inlet pressure was kept at $\sim 5 \times 10^{-7}$ mbar, whereas the inlet pressures of CO₂ and water were varied according to the desired ratio. After deposition at 10 K, this mixed ice was slowly heated (heating rate = 2 K.min⁻¹) up to 160 K and temperature dependent RAIR spectra were recorded. The gas composition was checked using the RGA.

RAIR spectra were recorded using a Bruker FT-IR spectrometer, Vertex 70. The external IR
25 beam was focused onto the substrate using gold plated mirrors through ZnSe windows (transparent to IR beam), attached to the vacuum chamber. The reflected IR beam from the substrate was re-focused using another gold-plated mirror to a liquid N₂ cooled external MCT (Mercury Cadmium Telluride) IR detector. The spectra were collected in the 4000-550 cm⁻¹
30 range with 2 cm⁻¹ resolution. Each spectrum was an average of 512 scans to get a better signal to noise ratio.

The clathrate hydrates were further characterized by temperature programmed desorption-mass spectrometry (TPD-MS) analysis. For this analysis, after ice deposition or clathrate hydrate formation, the substrate was moved to a fixed position by using the sample manipulator in order to ensure that the surface is close to the mass spectrometer inlet. During TPD-MS measurement, the substrate was heated at a constant heating rate ($30 \text{ K}\cdot\text{min}^{-1}$). Suitable mass of the desorbed species was selected by the RGA and the intensity of the desorbed species was plotted as a function of substrate temperature. Mass spectrometers were supplied by Extrel CMS, USA. For TPD, the inlet of the mass spectrometer was positioned 50 mm from the center of the Ru substrate.

10 **Computational details**

The stability of clathrate hydrate cages and their CO_2 , CH_4 inclusion complexes are examined computationally. All the considered cages of clathrate hydrates have been fully optimized at the B3LYP/6-311++G (d, p) level of theory using the Gaussian 09 program package. Frequency calculations characterize the obtained stationary points as minima on the potential energy surface. The sequentially added CO_2 and CH_4 molecules in 5^{12} , $5^{12}6^2$, and $5^{12}6^4$ clathrate hydrate cages and probed their cage occupancy. In general, the optimizations of clathrate hydrate cages were found to be quite challenging with the Gaussian programs. Normally, most optimizations of clathrate cages take a large number of steps and it was difficult to reach convergence. The B3LYP/6-311++G (d, p) level of theory was found to be reasonable for optimizations of clathrate hydrates and various other water clusters. The quantum theory of atoms in molecules (QTAIM) methodology was capable of revealing bonding interactions between individual functional groups and atoms in a molecule by the electron density distribution analysis.

All possible cages were considered in the present study. It was found that the 5^{12} clathrate hydrate cages were more stable; stability also depended on the size of the guest molecule. These results were also compared with the computational studies reported.

Results and Discussion

Figure 1 shows CH_4 hydrate formation as studied by RAIR spectroscopy and quantum chemical calculations. (A) Normalized time dependent RAIR spectra of 300 MLs $\text{CH}_4+\text{H}_2\text{O}$ (1:1) mixed ice at 10, 20, and 30 K at the C-H antisymmetric stretching region. (B) Time dependent RAIR spectra of the same system at 30 K. Here, the blue trace was divided by a factor

of 7 to match the intensity of orange trace. Difference in intensity is due to desorption of CH₄ at 30 K, near its desorption temperature. Deconvoluted IR peaks are shown by cyan (3009 cm⁻¹) and pink shade (3017 cm⁻¹). (C) DFT-optimized structure of CH₄ trapped within CH (5¹² cage). Here, water cage and guest molecule (CH₄) are shown. Color code used: gray, C; red, O; cyan, H.

5 Figure 1A displays time-dependent reflection absorption infrared (RAIR) spectra of 300 MLs (MLs = monolayers; 1 monolayer is equivalent to $\sim 1.0 \times 10^{15}$ molecules.cm⁻²) of a co-deposited mixture (1:1) of CH₄ and water at the C-H antisymmetric stretching region, at 3 different temperatures (10, 20, and 30 K) and two different annealing times (0 and 25 h), under UHV. The annealing time is crucial for the success of the experiment. The figure clearly shows
10 no change in peak position for the C-H antisymmetric stretching band of solid CH₄ (3009 cm⁻¹) with time, at 10 and 20 K. This peak is due to the untrapped CH₄, in other words, CH₄ hydrate was not observed at 10 and 20 K. A completely new IR peak (3017 cm⁻¹) appears alongside the peak at 3009 cm⁻¹ after 25 hours of annealing at 30 K. This new peak (3017 cm⁻¹) is attributed to the CH₄ hydrate, where CH₄ is trapped in the CH cage. The rest of the untrapped CH₄ remained
15 in the pores of amorphous ice. The experimental blue shift of 8 cm⁻¹ is due to the entrapment of CH₄ in the hydrate cage. Here, the trapped CH₄ inside CH cage behaves more like gaseous CH₄ as expected. It is known that vibrational frequency of free guest molecules in CH fall in between their vapor and condensed phase frequencies. The IR peak was deconvoluted to show the actual concentration of CH₄ trapped inside the hydrate cages and pores of amorphous solid water
20 (ASW). The peak widths were calculated upon deconvolution, and the values were, 14.1 and 4.2 cm⁻¹ for the peaks at 3009 and 3017 cm⁻¹, respectively. Note the reduced width (4.2) of 3017 cm⁻¹ for the hydrate peak, characteristic of a unique structure. Taking the IR intensity, the extent of CH₄ in the hydrate form was estimated to be 12.71% of the total CH₄ at this condition. As the annealing temperature is close to that of desorption, about 6/7th of the adsorbed CH₄ desorbs
25 during annealing. Furthermore, confirmed the formation of CH₄ hydrate by quantum chemical calculations. DFT calculations of the CH₄ hydrate revealed that the small cage (5¹²) as shown in Figure 1C is favorable to form at this particular condition. Computationally determined shift in the C-H antisymmetric mode during hydrate formation closely matches with the experimental value (Table 1). A micro-second molecular dynamics simulation of CH₄ hydrate nucleation
30 predicts preferential formation of smaller 5¹² cages in the initial stages of CH₄ hydrate nucleation, supporting the observation.

Keeping, CH₄ and water ice mixture at 30 K for more than 25 hours results in the formation of CH₄ hydrate. The long experimental time scale and the temperature (30 K), very near to the desorption temperature of CH₄, are two crucial factors for the formation of CH₄ hydrate under UHV conditions. The prolonged subjugation of CH₄-water mixture at 30 K, enhances the mobility of CH₄ molecules and leads to its insertion within the cages formed simultaneously. In a time-dependent study of 150 MLs of pure solid CH₄ at 25 K (Figure 5), the additional peak (3017 cm⁻¹) was not observed. This is again an evidence that the above peak is due to CH₄ hydrate.

To support the formation of CH in ISM, the present invention have chosen a more stable hydrate, namely CO₂ which is already known to form CH at 120 K and 10⁻⁶ torr.

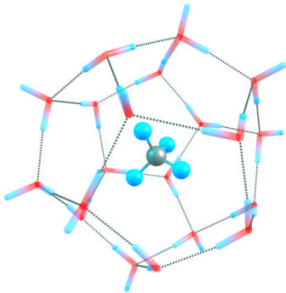
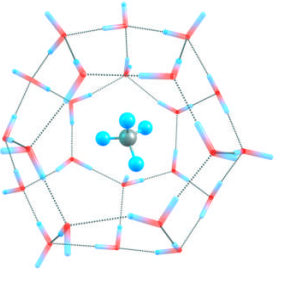
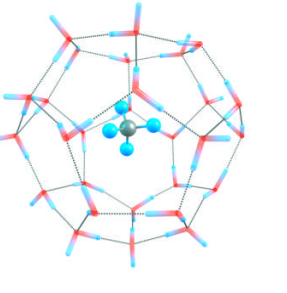
Figure 2 shows CO₂ hydrate formation as studied by RAIR spectroscopy and quantum mechanical calculations. (A) Normalized temperature dependent RAIR spectra of 300 MLs CO₂+H₂O (1:5) mixed ice at C=O antisymmetric stretching region. A new peak at 2346 cm⁻¹ arises due to the formation of CO₂ hydrate. (B) Ratio dependent RAIR spectra of 300 MLs CO₂+H₂O at 10 K (normalized). (C) DFT-optimized structure of CO₂ trapped inside CH (5¹² cage). Here, water cage and guest molecule (CO₂) are shown. Color code used: gray, C; red, O; cyan, H.

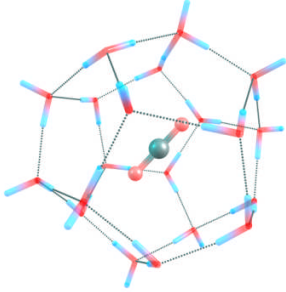
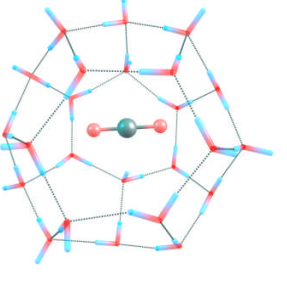
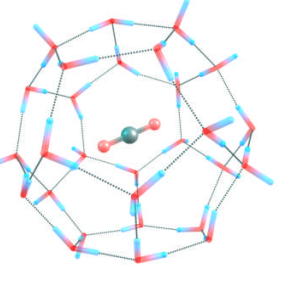
Figure 2A represents the temperature-dependent RAIR spectra of 300 MLs of the co-deposited mixture (1:5 ratio) of CO₂ and water in the C=O antisymmetric stretching region. The figure shows two IR peaks for the C=O antisymmetric stretching band of solid CO₂ at 10 K. The peak at 2353 cm⁻¹ is attributed to the untrapped CO₂ which exists outside of the CH cage, and in the amorphous pores of water-ice. The other peak, positioned at 2346 cm⁻¹ is due to the CO₂ entrapped in the CH cage. Now, as the system was annealed further to 50 K (heating rate=2 K.min⁻¹), the intensity of the CO₂ hydrate peak (2346 cm⁻¹) increased and that of the free CO₂ peak (2353 cm⁻¹) decreased. At 120 K, the untrapped CO₂ peak vanished completely and only the CO₂ hydrate peak remained. It indicates that the annealing of CO₂ mixed ice leads to the gradual formation of CO₂ hydrate and the transformation is complete at 120 K. Furthermore, no change in CO₂ hydrate peak position (2346 cm⁻¹) was observed when the system was kept at 120 K for 6 hours (Figure2A). This confirms that the CO₂ hydrate is quite stable in these analogous astrochemical conditions. It is also clear that CO₂ hydrate forms even at 10 K during deposition itself.

The stoichiometric ratio of water and guest molecules is an essential aspect of controlling the formation of CH. The ideal ratio of water and guest molecules is 20:1 for CH₃OH hydrate formed at 130 K and at 10⁻⁶ torr pressure. Figure 2B shows the comparative formation of CO₂ hydrate at different ratios of CO₂:H₂O at 10 K under UHV. The figure clearly indicates that the intensity of 2346 cm⁻¹ peak is maximum for a 1:90 mixture as compared to the other ratios. This suggests the optimum ratio needed for CO₂ hydrate formation at 10 K, which is a very diluted mixed ice. The shoulder at 2353 cm⁻¹ vanished upon keeping the ice at 10 K for over 48 hours as shown in Figure 2B, suggesting that all the remaining free CO₂ forms hydrate structure over time.

The formation of CO₂ hydrate is confirmed by quantum chemical calculations. These calculations revealed that the small cage (5¹²) as shown in Figure. 2C, is favorable to form. The computationally determined shift in the C=O antisymmetric mode closely matches with the experimental vibrational shift upon hydrate formation. Here, CO₂ is interacting with the water cage through hydrogen bonding, and consequently, there is a red shift. This result agrees well with the experimental shift (Table 1). Other possible cages computed (5¹²6² and 5¹²6⁴) have reduced or opposite shift, respectively (Table 1).

Table 1 Comparison of the computational and experimental vibrational shift of CH₄ and CO₂ clathrate hydrate compared to free CH₄ and CO₂ using the B3LYP level of theory with 6-311++G (d, p) basis set. Optimized structures are shown.

	5 ¹² cage	5 ¹² 6 ² cage	5 ¹² 6 ⁴ cage
CH₄ Clathrate hydrate			
Experimental shift	8.0 cm ⁻¹	-	-

Computational shift	9.3 cm ⁻¹	-9.2 cm ⁻¹	-9.1 cm ⁻¹
CO₂ Clathrate hydrate			
Experimental shift	-36.0 cm ⁻¹	-	-
Computational shift	-86.0 cm ⁻¹	-16.6 cm ⁻¹	15.8 cm ⁻¹

The rapid formation of CO₂ hydrate as compared to the slow kinetics seen for CH₄ hydrate is because of the induced polarity of CO₂. Nucleation mechanism of CH formation varies for different guest molecules and can depend on their chemical nature. During the nucleation of CO₂ hydrate structure, it interacts with water through stronger interaction, whereas, CH₄ is unable to interact similarly. The analysis is extended using Bader's theory of Atoms in Molecules (AIM) in order to confirm the nature of interaction of guest molecules with hydrate cages. The electron density $\rho(\mathbf{r}_C)$ values obtained for the critical points between a particular atom of the guest species and the hydrate cage along with the corresponding Laplacian of the electron density ($\nabla^2\rho(\mathbf{r}_C)$) are listed in (Table 2). The higher value of electron density ($\rho(\mathbf{r}_C)$) for the critical point between the O atom of CO₂ and the hydrate cage (0.01563a.u.) compared to that between the H atom of CH₄ (0.00598a.u.) and the hydrate cage suggests that the interaction for CO₂ is stronger than that for methane. The clathrate hydrates of other guest molecules, such as tetrahydrofuran (THF) and acetone hydrate can also be formed.

Table 2 Properties of (3,-1) bond critical points in CH₄ and CO₂ clathrate hydrate computed at B3LYP level of theory with 6-311++G (d, p) basis set.

Clathrate Hydrate	Type of bonding	Bonds	$\rho(\mathbf{r}_C)$	$\nabla^2\rho(\mathbf{r}_C)$
--------------------------	------------------------	--------------	----------------------	------------------------------

(⁵¹²)				
CH ₄	van der Waals interaction	-C-H of free CH ₄	0.27217	-0.89913
		-C-H of CH ₄ hydrate	0.27199	-0.89544
		-C-H··H ₂ O interaction	0.00598	0.01601
CO ₂	Hydrogen bonding	-C=O of free CO ₂	0.45773	-0.08650
		-C=O of CO ₂ hydrate	0.44922	-0.07620
		-C=O··H ₂ O interaction	0.01563	0.07161

In the previous experiments, co-deposition of CO₂ and water results in CH. Sequential deposition was also carried out. Annealing of this sequentially deposited system; CO₂@H₂O (1:5 ratio), did not result to CO₂ hydrate and the 2346 cm⁻¹ peak was not observed (Figure 6). Here, the peak at 2381 cm⁻¹ is attributed to pure multilayer CO₂. This phenomenon strongly supports the fact that proper mixing of water and CO₂ is a crucial step for the formation of CO₂ hydrate. The co-deposition method allows better mixing of CO₂ molecules with water where as sequential deposition does not. Sequential deposition of water over CO₂ may result in diffusional mixing but this does not lead to the formation of CH.

About 1% of ¹³CO₂ is present along with ¹²CO₂ naturally as shown (Figure 7). During the ¹²CO₂ hydrate experiment, ¹³CO₂ also shows CH upon annealing to 120 K. Temperature-dependent RAIR spectra in the ¹³C=O antisymmetric stretching region (Figure 8), where the 2282 cm⁻¹ peak is due to untrapped ¹³CO₂, and that at 2278 cm⁻¹ is due to ¹³CO₂ hydrate.

Figure 3 shows TPD mass spectra of 300 MLs of co-deposited ice systems at different ratio (heating rate 30 K min⁻¹). Here, the intensities of CH₃⁺ (m/z = 15), and CO₂⁺ (m/z = 44) are plotted. (A) Desorption of CH₄ after hydrate formation (magenta line), and before hydrate formation (blue line). MV peaks are shown in the insets. Peaks labelled * are attributed to desorption due to structural transitions of ASW upon annealing. (B) Desorption of CO₂ after hydrate formation at different ratios, as indicated. The peak labelled # is due to the pre-dissociation of CO₂ hydrate cage. (C) Schematic representation of MV upon crystallization of ice.

The formation of CHs in ISM condition is further confirmed by temperature programmed desorption-mass spectrometry (TPD-MS). The trapped guest molecules within ASW are released

when amorphous to crystalline ice transition occurs at 140 K. Figure 3A represents the comparative TPD spectra before and after the formation of CH₄ hydrate. The spectra correspond to CH₄ desorption and were monitored using the intensity of CH₃⁺ alone. Peaks at 38 K and 46 K correspond to multilayer CH₄ and CH₄ trapped in ASW (CH₄·ASW), respectively. These TPD peaks are assigned by a control study as shown (Figure 9). The CH₄ hydrate was formed by annealing a co-deposited mixture at 30 K for 25 hours, and during this course, most of the free CH₄ got desorbed, as observed from TPD. Desorption of CH₄ in trapped ASW got shifted to 53 K after the formation of CH. The abrupt release of trapped gases from ASW at 140 K is termed as molecular volcano (MV). The intensity of MV peak (at 140 K) increases, upon the formation of CH₄ hydrate. Before the formation of CH₄ hydrate, the MV peak is due to the trapped CH₄ in ASW. The reason for the enhancement of MV peak intensity is the simultaneous release of trapped CH₄ from ASW pores as well as from the CH₄ hydrate cage (Figure 3C). Note that the amount of gases deposited is the same in both the cases. Slight distortion in the MV peak is attributed to the modification of ASW pores due to CH formation (Figure 3A). The amount of desorption due to CH is estimated to be 14.53% of the total CH₄ at this condition and it is correlated to the amount of CH calculated from the IR data (Figure 1B).

In Figure 3B, comparison of the TPD spectra of 300 MLs of CO₂+H₂O at two ratios; 1:1 and 1:5, which were deposited at 10 K. Then, these two systems were annealed at 120 K for the complete formation of CO₂ hydrate. After that, they were cooled back to 10 K, and TPD mass spectra were taken. The heating rate for TPD was 30 K min⁻¹. The peak at 140 K corresponds to MV of CO₂. Figure 3B shows that the intensity of MV increased as the ratio of CO₂ and H₂O was changed from 1:1 to 1:5. Taking the area under the MV peaks, the amount of CH formed was found 1.7 times higher for (1:5) than the former. As previously explained, the extent of formation of CO₂ hydrate is greater for the latter ratio (Figure 2). Here again, the enhancement agrees with the IR data. No additional desorption of CH₄ and CO₂ above this temperature suggest that the hydrates have been decomposed. The cubic crystalline ice can be formed via acetone hydrate under ultrahigh vacuum and at 130-135 K.

Figure 4 shows equilibrium curve for CH₄ clathrate hydrate. The curve depicts the stability of CH₄ clathrate hydrate as a function of temperature and pressure. Extrapolation of the curve to 30 K, denotes that CH₄ hydrate could be stable up to 2×10⁻⁶ mbar pressure. Two different pressure zones of the equilibrium curve are indicated with different colours.

In Figure 5 time dependent RAIR spectra of 150 MLs of solid CH₄ in the C-H antisymmetric stretching region at 25 K is illustrated. The decrease in the intensity of the IR peak is due to desorption of CH₄ in UHV. This experiment was performed at 25 K instead of 30 K, as at this temperature (30 K), most of the CH₄ desorbed from the surface after 30 hours.

5 Figure 6 shows temperature dependent RAIR spectra of 300 MLs of CO₂@H₂O (1:5 ratio) in the C=O antisymmetric stretching region. Spectrum for pure solid CO₂ was added for comparison. The CO₂@H₂O symbolism implies that H₂O was deposited over CO₂. The spectra were translated vertically for the clarity. Full scale RAIR spectrum of 300 MLs of CO₂+H₂O (1:5 ratio) at 10 K (Figure 7). Temperature dependent RAIR spectra of 300 MLs of CO₂+H₂O (1:5 ratio) in the 13C=O antisymmetric region (Figure 8). Reduction in intensity with time is due to partial desorption.

TPD mass spectra of 150 MLs of solid CH₄ and CH₄+H₂O co-deposited ice systems at different ratios (heating rate of 30 K.min⁻¹) is illustrated in Figure 9. Here, the intensities of CH₃⁺ (m/z=15) under these conditions are plotted. After the deposition at 10 K, these ice systems were annealed and simultaneously the mass spectra were recorded. The marked desorption (*, \$) peaks are due to the structural transitions of amorphous ice during annealing.

Example 2

20 **Formation of cubic ice via acetone clathrate hydrate, prepared in ultrahigh vacuum under cryogenic conditions Experimental Section**

Experiments were carried in an ultrahigh vacuum (UHV) chamber (base pressure $\sim 5 \times 10^{-10}$ mbar). This kind of low pressure is an essential condition for simulating the ISM or cometary environments. The vacuum was maintained by several oil-free turbo molecular pumps backed by diaphragm pumps (Pfeiffer Vacuum). In brief, the chamber was equipped with reflection absorption infrared (RAIR) spectroscopy and temperature-programmed desorption (TPD) mass spectrometry. Here, a Ru(0001) single crystal was used as the substrate. A thin film of ice was grown on top of this substrate, mounted on a copper holder, which in turn, was attached at the tip of a closed cycle helium cryostat (Cold Edge Technologies). The temperature was measured by using a K-type thermocouple connected to it. Repeated heating at 400 K before vapor deposition ensured surface cleanliness. The temperature ramping was controlled and monitored by a temperature controller (Lakeshore 336).

Acetone hydrate was formed by using ~99.99% pure acetone, purchased from Sigma-Aldrich and Millipore water (H₂O of 18.2 MΩ resistivity), taken in separate test tubes, connected to the sample line through a glass-to-metal seal. Here, both acetone and water were additionally purified through several freeze-pump-thaw cycles before introduction into the experimental chamber. The sample lines were connected to the experimental chamber through a high precision all-metal leak valve. These leak valves were used to control the flow or inlet pressure of different samples. Out of the two sample inlet lines, one was exclusively used for acetone while the other line was used for water deposition. During the exposure of different samples into the UHV chamber, their purities were checked using a quadrupole mass spectrometer (Extrel) installed in the chamber. Recorded mass spectra were used to monitor purity as well as to measure the ratio of the mixtures. The ratio of the mixed ice was determined by controlling the flow or inlet pressure of the sample. Here, we express the film thickness in terms of the monolayer (ML), assuming that 1.33×10^{-6} mbar.s = 1 ML which has been estimated to contain $\sim 1.1 \times 10^{15}$ molecules.cm⁻². A number of reports adopted this calculation for the estimation of surface coverages. The inlet pressure during sample deposition was decided based on the coverage desired at the time of the experiment. The substrate was kept in a fixed perpendicular position for uniform growth of ice. For accurate estimations, the relative sensitivities of ion gauge response (ion gauge coefficient) towards different molecules have to be accounted.⁵ Other ways of estimating coverage include determination of molecular flux by Hertz-Knudsen equation, numerical integration of thermal desorption spectra.⁶ Despite this limitation, the present method was chosen for its simplicity. A 1:1 monolayer mixture of acetone:H₂O will be 3.22:1 in molar ratio. However, it is difficult to estimate the actual ratio (acetone:H₂O) during the nucleation of acetone hydrate at higher temperature, due to the desorption of acetone. The nucleation is primarily governed by the annealing temperature and residence time.

Here, to prepare 300 MLs of acetone:H₂O (1:1), the UHV chamber was backfilled at a total pressure of $\sim 5 \times 10^{-7}$ mbar (where, acetone inlet pressure = 2.5×10^{-7} mbar, and water inlet pressure = 2.5×10^{-7} mbar) and deposition was continued for 10 minutes. Now, this mixed ice was slowly (heating rate = 2 K.min⁻¹) heated to the required experimental temperatures (120, 130, and 135 K). At these temperatures, the mixed ice was monitored constantly by RAIRS with time. For decoupled O-D stretching analysis, the samples were prepared using D₂O (~5%) in H₂O. In this solution, D₂O undergoes H/D exchange to form HDO. The use of HDO facilitates the

observation of ASW crystallization because the O-D stretching vibration is decoupled from intramolecular and intermolecular O-H stretching vibrations.

RAIR spectra were recorded using a Bruker FT-IR spectrometer, Vertex 70. The external IR beam was focused onto the substrate using gold plated mirrors through ZnSe flanges (transparent to IR beam), attached to the vacuum chamber. The reflected IR beam from the substrate was re-focused using another gold-plated mirror to a liquid N₂ cooled external MCT IR detector. The spectra were collected in the 4000-550 cm⁻¹ range with 2 cm⁻¹ resolution. Each spectrum was averaged for 512 scans to get a better signal to noise ratio.

The CHs produced in the UHV condition were further characterized by temperature programmed desorption-mass spectrometry (TPD-MS) analysis. For TPD-MS, after ice deposition or clathrate hydrate formation, the substrate was moved to a fixed position by using a sample manipulator to ensure that the surface is very close to the mass spectrometer inlet and the substrate was ramped at a constant heating rate (30 K.min⁻¹). Suitable masses of the desorbed species (m/z = 43 for acetone, m/z = 18 for H₂O) were selected by a linear quadrupole mass spectrometer analyzer, and the intensity of the desorbed species was plotted as a function of substrate temperature. Extrel CMS, USA supplied the mass spectrometers.

Reflection high-energy electron diffraction (RHEED) study was carried out in a different UHV chamber of base pressure $\sim 1.33 \times 10^{-10}$ mbar, which was described in detail elsewhere. To obtain RHEED patterns, we used a focused high-energy electron beam (30 keV) that was generated by an electron gun (Eiko Co. Ltd., MB-1000). The diffraction pattern projected onto a phosphor screen was recorded using a high-sensitivity CCD camera intermittently (pulse duration of ~ 0.5 s), only at specific temperatures and coverages of interest to reduce sample damage. The typical electron beam current during the RHEED measurement was 5-7 nA, as determined using a Faraday cup. The spot size and glancing angle of the beam were 0.1 mm and 2-3°, respectively.

Acetone hydrate formed in UHV could transform into ice I_c upon in-situ dissociation of the former at 130-135 K. Ice I_c via acetone hydrate was prepared by annealing a co-deposited ~ 300 MLs acetone:H₂O (1:1) film to 135 K and maintaining it there in UHV for 3 hours (additional experimental details are given in supporting information). Figure 10 shows the RAIR spectra obtained immediately after annealing the co-deposited film at 135 K (blue trace; 0 h), and after 3 hours (orange trace; 3 h). Inset of Figure 10 shows the time-dependent RAIR spectra of the same system in the C=O stretching region. In Figure 10, only the O-H (2800-4000

cm⁻¹) and C=O (1650-1770 cm⁻¹) stretching regions were displayed as these two regions are important for the acetone:H₂O system where major changes were observed. At 135 K, the O-H bending band became featureless, and therefore, it was neglected in the spectra. The C=O stretching band at 0 h shows two features at ~1721 and ~1709 cm⁻¹, which are attributed to acetone hydrate and ASW-trapped acetone, respectively based on previous IR studies. These two features were deconvoluted to predict the actual amount of acetone in the hydrate form with respect to the total acetone present. Taking the area under the 1721 cm⁻¹ peak, the amount of acetone in the hydrate form was estimated to be 32.59% of the total acetone. Isothermal time-dependent RAIR spectra of 150 MLs of pure acetone, measured at different temperatures (115, 120, and 125 K) showed a major feature at ~1718 cm⁻¹ due to bulk acetone. This confirmed that 1721 cm⁻¹ peak is entirely a new feature and arises only due to acetone hydrate and not due to bulk acetone or its aggregates. However, it is not stable in this condition, and dissociated within 3 hours. Inset of Figure 10 shows the reduction of C=O stretching band with time and resulted in a weak feature at ~1702 cm⁻¹. This feature is assigned to a dilute mixture of acetone and water (1:20), which was separately examined.

Acetone is a relatively less abundant molecule in the cometary environment. The performed time-dependent RAIR spectra for dilute mixtures (1:10 and 1:20) of acetone:H₂O at 135 K. They also resulted in ice I_c in processes as described. Therefore, it is confirmed that acetone hydrate could be formed even with a very dilute mixture of acetone:H₂O which may have direct relevance from the cometary science perspective. However, to present the results in a clear and consistent way, a 1:1 mixture was used which allowed us to obtain better quality spectra and monitor the changes distinctly in the spectra.

The O-H stretching band also underwent a profound change with time. The featureless broad O-H stretching band at 0 hour is a characteristic feature of ASW (blue trace in Figure 10). However, this particular band is red-shifted with respect to the O-H stretching band of an ASW film, reflecting the increase in the order and number of H-bonded water molecules with time. The unit cells of hydrates are complex, and the water molecules reside in several in equivalent sites which results in the broadening of the O-H stretching band of the host ice network. This band became sharp and got split partially after 3 hours (orange trace in Figure 10). Splitting and sharpening of O-H stretching of the IR spectrum are associated with the crystallization of the ice film. This O-H band was deconvoluted to three distinct features as shown in Figure 10. The

features at 3164, 3284, and 3395 cm^{-1} correspond to ν_1 in-phase band, ν_3 TO band, and the overlapped ν_3 LO and ν_1 out-of-phase bands of ice I_c . These assignments were made based on the previous IR studies of ice I_c . It is evident that acetone hydrate in UHV slowly (within 3 hours) dissociates at 135 K, leading to ice I_c . A similar time-dependent RAIR study of the same system is carried out at 130 and 120 K. The acetone hydrate is formed at 130 K got converted to ice I_c after 9 hours. However, the formation of acetone hydrate and subsequent crystallization to ice I_c were not observed at 120 K, even after 48 hours. This observation indicates that the thermal motion of acetone molecules is responsible for the formation of acetone CH. At low temperature (≤ 120 K), these motions are restricted, however, they became significant near the acetone desorption temperature (~ 130 K) in UHV. Earlier studies also suggest that molecular mobility plays a vital role in the entrapment of guest molecules into the hydrate cages; therefore, temperature near desorption of guest species used here is crucial for the observed phenomenon.

A similar time-dependent study was carried out with 300 MLs of acetone: D_2O (1:1) at 140 K and cubic D_2O ice was formed upon dissociation of acetone hydrate. The requirement of slightly higher temperature of 140 K is understandable since D_2O is a heavier molecule than H_2O , whose rearrangement required a higher temperature.

Thin films of ASW (< 30 MLs) grown by vapor deposition below 110 K is known to have intrinsic ferroelectricity and negative surface potential. However, in this study, contribution of these effects of ice may be disregarded, since all the experiments were performed with higher coverage of ice (300 MLs) and above 120 K when such properties disappear. Time-dependent studies of pure 150 MLs of H_2O were carried out at 120 and 130 K, and self-crystallization of ice was not observed. It proved that dissociation of acetone hydrate alone produced the ice I_c , even at a lower temperature.

Structure of ice formed is crucial to be investigated by more direct measurements. Figure 11 shows the time-dependent reflection high-energy electron diffraction (RHEED) images of 300 MLs of acetone: H_2O (1:1) at different temperatures as indicated. These experiments were conducted in a separate chamber, by depositing 300 MLs of mixed ice on Ni (111) substrate at 20 K. After deposition, the mixture was annealed (heating rate = 2 $\text{K}\cdot\text{min}^{-1}$) to the experimental temperatures and kept for the required time, as shown in the figure. Here, it must be noted that all of the experiments were performed under multilayer deposition conditions, and therefore, the substrate does not play a role in the morphology of the deposited ice systems. The RHEED

image in Figure 11a, which was taken immediately after annealing the acetone:H₂O system at 135 K does not show any pattern indicating the amorphous nature of the mixture. However, after 5 hours, several diffraction rings were observed (Figure 11b). Notably, these diffraction patterns originate from the water ice film. In this particular condition, most of the acetone molecules desorb from the mixture as indicated by the IR measurement. The RHEED pattern indicates that the water film is ordered, *i.e.*, this is a crystalline ice film which is cubic, as the observed diffraction patterns match with the earlier diffraction studies of ice I_c. Time-dependent RHEED experiments were carried out at 130 and 120 K as well. We observed in Figure 11d that after 12 hours at 130 K, the ice became cubic. However, at 120 K, the ice I_c diffraction patterns were not observed, even after conducting the study for 24 hours (Figure 11e and 11f). These observations are in accordance with the RAIR spectra presented in Figure 10. From an analysis of the diffraction patterns in Figure 11, it is evident that ice I_c was formed only through the dissociation of acetone hydrate.

Figure 12 shows the TPD-MS spectra of 300 MLs of acetone:H₂O (1:1). Here, the ice film was heated at 30 K.min⁻¹ to obtain the TPD spectra. In Figure 12a, for the desorption trace of acetone, the intensity of CH₃CO⁺ (m/z = 43) is shown as a function of temperature. It shows a sharp desorption feature at 134 K, due to the dissociation of untrapped acetone which exists outside the hydrate cage. It was further confirmed by the TPD of pure acetone which shows desorption peak at 132 K. It is to be noted that acetone starts to form hydrate just by annealing to 130 K as shown in Figure 12. In TPD, the shoulder marked with \$ is due to acetone hydrate dissociation. This feature of acetone (Figure 12a) may have a contribution from the molecular volcano (MV) of acetone as it coincides with the transition of ASW to crystalline ice transition (Figure 12b). Deconvoluting the desorption trace of acetone, the amount of desorption due to acetone hydrate is estimated to be 24.26% of the total acetone at this condition, and it is correlated to the amount of acetone in hydrate form calculated from the IR data (Figure 10). This smaller amount of acetone is also observed in the RAIRS study as shown in Figure 10 where a weak feature at ~1702 cm⁻¹ was observed even after hydrate dissociation, which was further confirmed in a separate experiment. The desorption trace of H₂O⁺ (m/z = 18) consists of two features as shown by spectral deconvolution. The vapor pressure (desorption rate) of ASW is higher than crystalline ice, which resulted in a bump shown by pink shade. Interestingly, this bump occurs

right at the same temperature when acetone hydrate dissociated. Therefore, this is another evidence to suggest that dissociation of acetone hydrate resulted in the crystallization of ice.

The time-dependent RAIR spectra of acetone:HDO (5% D₂O in H₂O) at different temperatures (130, 135, 132, and 137 K). In Figure 13a, the bottom most spectrum (0 h trace) indicates a pure ASW film which got crystallized with time. Evaluated the crystallization fraction, $x(t)$ from changes in the absorbance (ΔA) at a fixed wave number (3307 cm⁻¹ in Figure 13a, indicated by the vertical line) for each temperature. Also in Figure 13b, the initially broad amorphous spectrum (0 min trace) eventually got transformed into a relatively sharp crystalline spectrum with a peak at ~2427 cm⁻¹. Here, differences in the integrated peak area between the completely ASW and (partly) crystalline films at each time interval were considered. However, changes in the absorbance (ΔA) at a fixed wave number (~2427 cm⁻¹ in Figure 13b, indicated by a vertical line) produced almost the same result for $x(t)$ as that obtained from the integrated peak area. The crystallization fraction was calculated by equation 1,

$$x(t) = \frac{\Delta A(1)}{\Delta A(2)} \quad (1)$$

where, $\Delta A(1)$ is the difference in the absorbance at a particular time ' t ' and that at time zero; $\Delta A(2)$ is the difference in absorbance of completely crystallized film and that at time zero.

Figures 14a and 14b illustrate the changes in the crystallization fractions as measured from the O-H and decoupled O-D stretching bands, conducted at different temperatures as shown. It was evident that the rate of crystallization was increased with rise in temperature. This change was reflected in the change of the curve shape from sigmoidal to exponential, with temperature. Next, the crystallization fraction at different temperatures were fitted to the Avrami equation,

$$x(t) = 1 - \exp[-k(T).t]^n \quad (2)$$

where t is time, $k(T)$ is the rate constant, and n is the Avrami exponent. For all temperatures, n is a parameter whose value indicates the geometry of the growing particles and the type of nucleation, whether it is diffusion or interface controlled. Thus, the nature of the crystallization process can be predicted from the knowledge of Avrami exponent, n . After rearranging, this equation becomes,

$$\ln(-\ln[1-x(t)]) = n \ln(t) + n \ln k(T) \quad (3)$$

Figures 15a and 15b show linearly fitted straight lines using equation 3, for different temperatures as shown. The values of n are determined from the slopes. Using the values of n

and intercept of the straight lines for each temperature, the rate constants, $k(T)$ are estimated. Values of n and $k(T)$ obtained from the analysis of O-H and O-D stretching bands at different temperatures are summarized in Table 3.

Table 3 The parameters for crystallization of ice I_c during the dissociation of acetone hydrate at different temperatures.

	Temperature (K)	n	Rate constant; k (s^{-1})
O-H stretching	130	2.49	2.47×10^{-5}
	132	2.45	6.37×10^{-5}
	135	2.05	1.80×10^{-4}
	137	1.62	4.04×10^{-4}
O-D stretching	130	2.59	2.36×10^{-5}
	132	2.51	5.76×10^{-5}
	135	2.08	1.50×10^{-4}
	137	1.81	3.94×10^{-4}

The obtained values of n (2.59 to 1.62, in Table 3) suggest that the crystallization kinetics is diffusion-controlled with particles growing into a predominantly spherical geometry. Previous studies also suggest that the crystallization kinetics of water to ice I_c at $T < 150$ K is diffusion controlled with predominantly spherical growth. Here, we suggest that dissociation of acetone hydrate can promote the diffusion or mobility of H_2O molecules which essentially trigger the formation of crystalline ice. Figures 15c and 15d show the Arrhenius plot obtained from the analysis of the O-H, and the O-D stretching regions, respectively. The slope of these linearly fitted lines gave the activation energy (E_a), which were estimated to be ~ 57.92 and ~ 57.58 kJ.mol⁻¹, respectively. This is comparable to the previously reported activation energy values ($E_a = 60-77$ kJ.mol⁻¹) for the crystallization of pure ASW obtained by different experimental techniques. Here, the high mobility of the water molecules during hydrate dissociation can overcome the kinetic barrier to form crystals even at a lower than usual ice-crystallization temperature.

20

Example 3

Spontaneous formation of tetrahydrofuran hydrate in ultrahigh vacuum

Experimental section

The experiments were conducted in a UHV chamber with a base pressure of $\sim 5 \times 10^{-10}$ mbar. The UHV chamber has been described in detail elsewhere. Briefly, the chamber was equipped with RAIRS and temperature-programmed desorption (TPD) mass spectrometry. The substrate, a Ru(0001) single crystal, was cooled by a closed-cycle helium cryostat to 10 K. The substrate temperature was measured using a K-type thermocouple wire connected to it. The substrate was cleaned by heating to 400 K multiple times prior to vapor deposition. Desired molecular solid films were grown on Ru(0001) by vapor deposition at 10 K. The surface coverage of molecular solids was represented in terms of monolayers (MLs) assuming that 1.33×10^{-6} mbar.s = 1 ML which was estimated to contain $\sim 1.1 \times 10^{15}$ molecules.cm⁻². In a number of earlier reports, such calculation was used for the estimation of surface coverages. One point to be noted is that all the experiments were performed under multilayer deposition conditions, and therefore, the substrate does not play any role in the processes mentioned here.

THF (Sigma-Aldrich, 99%) and H₂O (Milli-Q, 18.2 MΩ resistivity) were purified by multiple freeze-pump-thaw cycles. The molecular solids of water and THF were prepared on a Ru(0001) substrate by sequential and co-deposition methods as per the need of the experiment. The vapors of THF and water were backfilled into the UHV chamber through variable all metal leak valves. For the deposition of 300 MLs of (1:5) mixed THF and water, the chamber was backfilled at a total pressure of $\sim 5 \times 10^{-7}$ mbar (where THF and water partial pressures were 1×10^{-7} , and 4×10^{-7} mbar, respectively, monitored by the mass spectrometer during deposition) and the mixture was exposed to the substrate for 10 minutes. To prepare other mixtures, the partial pressures of the individual components were set as per their requirement. The deposited mixed ice was slowly annealed (heating rate = 2 K.min⁻¹) to 130 K and time-dependent RAIR spectra were recorded. RAIRS measurements were performed using a Bruker FT-IR spectrometer, Vertex 70 with a liquid-nitrogen cooled mercury cadmium telluride (MCT) detector. The IR beam path outside the UHV chamber was purged with dry nitrogen gas. All RAIR spectra were collected in the 4000-550 cm⁻¹ range with 2 cm⁻¹ spectral resolution, averaged over 512 scans.

Computational details: The three most common cages of CHs were considered for calculations. Geometry optimizations for the water cages and the host-guest complexes were performed using the B3LYP method in conjunction with the 6-311++G (d, p) basis set. All the optimized

geometries in this work were confirmed to be minima in the potential energy surface by the absence of imaginary frequencies in vibrational frequency analysis. It was shown that this basis set produced quite well all the geometries, frequencies, and electric properties of THF hydrate. The electronic structure calculations were performed using the GAUSSIAN 09 program. The input configuration of the water cages were taken from our previous work and were subsequently optimized.¹³ The optimized structures corresponding to the 5^{12} , $5^{12}6^2$, and $5^{12}6^4$ cages are shown later. It was observed that the $5^{12}6^4$ THF hydrate cage was quite stable; stability also depends on the size of the guest molecule.

Results and Discussion

Formation of tetrahydrofuran (THF) hydrates in UHV, using reflection absorption infrared spectroscopy (RAIRS). The 1:5 mixtures of THF and water were co-deposited from their vapor phase to a precooled Ru(0001) substrate at 10 K inside a UHV chamber. Annealing the mixture to 130 K and keeping it for 6 hours led to the formation of THF hydrate. RAIRS was used to monitor hydrate formation. Evolution of THF hydrates showed temperature-dependent kinetics, which was established by carrying out time-dependent RAIRS study of similar systems at different temperatures. Time-dependent RAIRS study at 130 K also showed the formation of THF hydrate in the case of sequential deposition (THF@H₂O).

Figure 16a shows the RAIR spectra of 300 MLs of a THF:H₂O mixture (1:5), which was co-deposited at 10 K on the Ru(0001) substrate. After deposition, it was slowly heated at 2 K.min⁻¹ to 130 K and kept at this temperature for 6 hours. Water is known to have orientational freedom at this temperature. Due to such motions, molecular organization can occur in the process of annealing. Isothermal annealing for extended periods of the order of the tens of hours was essential to form hydrates of methane at cryogenic conditions. The RAIR spectrum was measured immediately after heating to 130 K, which represents the 0 hour spectrum. The asymmetric C-O stretching band of THF showed two peaks at ~1034 and ~1053 cm⁻¹ which was due to THF trapped in different sites of ASW. The shoulder at 1070 cm⁻¹ converted gradually to a new peak at ~1074 cm⁻¹ after 6 hours at 130 K. This new peak is the characteristic feature of asymmetric C-O stretching of THF hydrate. It serves as a convenient indicator of THF hydrate since it lies well above the IR peak positions of other likely condensed phases of THF. Intensity of this new peak continued to increase over time while the intensity of other two peaks reduced gradually. After 6 hours, the intensity of this new peak reached a maximum whereas that of the

1034 cm^{-1} peak was reduced almost to zero. This suggests the conversion of THF hydrate from the ASW-trapped THF.

To check whether co-deposition was a prerequisite for hydrate formation, 150 MLs of THF were first deposited on Ru(0001) at 10 K, and subsequently, the film was covered with 150 MLs of H₂O. This sequential deposition is represented as, THF@H₂O. It was annealed at 2 $\text{K}\cdot\text{min}^{-1}$ to 130 K, and time-dependent spectra were collected as shown in Figure 17. The asymmetric C-O stretching region in Figure 17a shows IR features at 1066, 1053, and 1034 cm^{-1} at 0 hour at 130 K. These two peaks at ~ 1034 and ~ 1053 cm^{-1} are due to THF trapped in different sites of ASW, as explained earlier. Origin of the ~ 1066 cm^{-1} peak can be explained from temperature-dependent RAIR spectra of a THF@H₂O mixture (Figure 18a); where the same peak was observed at 90 K and beyond. The peak at ~ 1066 cm^{-1} is due to the formation of irregular THF crystallites. These crystallites form due to the diffusion of THF into the over layers of the ASW network, at ≥ 90 K. Pure THF undergoes crystallization at > 90 K.

In Figure 18b, at 90 K, the O-H stretching band shifts to a lower wave number, as indicated by the vertical bars of two different colors (green and orange). This again supports the formation of irregular THF crystallites within the ASW pores, which influences the ASW network.

Interestingly, the sequential deposition does not lead to the formation of THF hydrate just by annealing, as the characteristic peak (~ 1074 cm^{-1}) of the same was not observed in Figure 18a. However, the formation of THF hydrate was observed only when this THF@H₂O film was kept at 130 K for a few hours. The characteristic THF hydrate peak at ~ 1074 cm^{-1} started appearing with time and becomes more prominent after 6 hours. Alongside, the broad O-H stretching band also attained crystalline features with time. Diffusion of THF into the over layer ice network took place by annealing as explained before. After diffusion, a fraction of THF molecules got trapped as the ASW pores collapsed by annealing.

The effect of temperature on the formation of THF hydrate. Figure 19a and 19b show the time-dependent RAIR spectra of a 1:5 THF:H₂O mixture in the asymmetric C-O stretching region of THF at 120, and 125 K, respectively. In contour plots (Figure 19c & 19d), the intensities of peaks at 1053 and 1074 cm^{-1} are plotted to follow the hydrate formation. At 120 K, the rate of conversion of THF hydrate is so slow that even after 110 hours, it is incomplete (Figure 19a).

However, at 125 K, the rate of conversion is relatively faster as the 1074 cm⁻¹ peak showed substantial intensity within 38 hours. Earlier, we observed that it required not less than 6 hours at 130 K for substantial nucleation of THF hydrate. This demonstrates that the formation of THF hydrate is a temperature and time-dependent process, and it follows certain kinetics.

5 It was observed that the formation of THF hydrate was associated with the crystallization of ASW (Figure 16b and 17b) and the crystallization process showed both time and temperature-dependent kinetics. The progress of crystallization was followed monitoring the evolution of 1074 cm⁻¹ peak. Here, the intensity 1074 cm⁻¹ peak is proportional to the extent of clathrate formation which in turn is a measure of crystallization of the ice. Here, the Avrami equation is
 10 used to describes the extent of crystallization (y) as a function of time (t) during isothermal annealing at temperature T . The equation is,

$$y(T) = 1 - \exp[-k(T).t^n] \quad (4)$$

where t is time, $k(T)$ is the rate constant, and n is related to the crystallization mechanism. For all temperatures, n is a parameter whose magnitude is determined by the geometry of the growing
 15 particles and whether the transformation is diffusion or interface controlled. For an interface-controlled transformation, n is an integer from 1 to 4, depending upon the shape of the particle, whereas, in a diffusion-controlled transformation, n is usually a fraction except for the cylindrical geometry of the particle when it is equal to 1. Thus, the nature of crystallization process can be predicted from the knowledge of the parameter, n . To find out the values of n and
 20 $k(T)$ at different temperatures, the equation 1 can be rewritten as,

$$\ln(-\ln[1-y(T)]) = n \ln(t) + \ln k(T) \quad (5)$$

Figure 20a shows three linearly fitted straight lines corresponding to three different temperatures. These data points were obtained using equation 5, where the extent of crystallization (y) was assumed to be directly proportional to the intensity of the 1074 cm⁻¹ peak (THF hydrate), as
 25 explained before. The slope of each straight line corresponds to the value of n at different temperatures. The rate constants of the crystallization process, which in turn is the formation of hydrate at different temperatures, can be evaluated from the intercept values (from eqn. 5) of each straight line (Figure 20a). Once the rate constant is known at different temperatures, it is

possible to calculate the activation energy involved in the process. The values of n and the rate constants at different temperatures are given in Table 4. Here, the fractional values of n indicate that the crystallization process or the formation of CH is diffusion-controlled, as mentioned earlier. It is already known according to the criteria for the values of n , the crystallization kinetics of water at $T < 150$ K is diffusion-controlled.

Table 4: The parameters for crystallization of water during the formation of THF hydrate at different temperatures.

Temperature (K)	n	Rate constant; k (s^{-1})
120	0.64	2.64×10^{-4}
125	0.73	5.16×10^{-4}
130	0.88	1.57×10^{-3}

The experimental data as shown in Figure 20b were fitted to the Arrhenius equation. Slope of this line gives the activation energy (E_a), which was estimated to be $\sim 23.12 \text{ kJ.mol}^{-1}$. This is lesser than the previously reported activation energy (E_a) values ($60\text{-}77 \text{ kJ.mol}^{-1}$) for crystallization of pure ASW obtained by different experimental techniques. This considerably lower activation energy suggests the feasibility of the process; however, the process is kinetically hindered at such low temperature due to limited diffusion. At elevated temperature, due to thermal motion of the molecules, the entropy of the system is increased which in turn enhances the diffusion process and results in hydrate. At a temperature of 120 K or above, H_2O ice undergoes a structural change, and this temperature is very close to the desorption temperature of THF, therefore, these molecules also possess sufficient thermal motion. Combination of these two effects may be responsible for the formation of the hydrate. Due to hydrate formation, the system reaches a thermodynamically stable crystalline structure.

It would be interesting to know about the structures of THF hydrates which are formed at such low pressures. One would expect that the low-pressure hydrate can be structurally different from the conventional high-pressure hydrates. Unfortunately, our experimental set-up is not equipped with in-situ diffraction tools; neither has it had a set-up to transfer the sample for diffraction studies to get insight into the structural details. The crystalline forms (hexagonal and cubic) of ice were prepared separately by annealing 150 MLs of ASW to respective crystallization

temperatures. It was observed that O-H stretching of THF hydrate is similar in shape to hexagonal ice than that of cubic ice. We may conclude that during the formation of THF hydrate the overall ice is attaining a structure, comparable to the hexagonal ice. We note that THF hydrate is known to form s-II hydrate, which is cubic in nature. Computationally, optimized structures of THF entrapped in different CH cages (5^{12} , $5^{12}6^2$, and $5^{12}6^4$) are shown in Figure 21. These calculated structures revealed that a large cage ($5^{12}6^4$) is favored for the entrapment of THF, whereas the other two cages are unstable. Formation of THF hydrate around atmospheric pressure reveal that due to the large size of the THF molecule, it forms s-II hydrate structure and occupies the large cage ($5^{12}6^4$). Here, the computed shift in the C-O asymmetric mode of the $5^{12}6^4$ cage closely matches the experimental shift of the same (Table 5). Other possible cages computed ($5^{12}6$ and $5^{12}6^2$) have reduced or opposite shift, respectively (Table 5).

Table 5 Comparison of the computational and experimental vibrational shifts of THF clathrate hydrate. Computations were performed using B3LYP level of theory with 6-311++G (d, p) basis set.

THF clathrate hydrate	5^{12} cage	$5^{12}6^2$ cage	$5^{12}6^4$ cage
Experimental shift	-	-	19.0 cm^{-1}
Computational shift	3.2 cm^{-1}	-10.3 cm^{-1}	27.4 cm^{-1}

The present invention provides a suitable method to form spontaneous and stable THF hydrate at cryogenic conditions under UHV. The hydrate formation is found to be diffusion-controlled and is associated with the formation of the thermodynamically stable crystalline structure at lower than usual crystallization temperature of ice. Kinetic measurements reveal that the crystallization process at < 120 K is kinetically hindered due to limited motion of the guest and host molecules. However, upon achieving significant molecular motion or mobility at a warmer temperature (near 130 K or above), both THF and water molecules rearrange themselves to form the more stable hydrate structure.

It may be appreciated by those skilled in the art that the drawings, examples and detailed description herein are to be regarded in an illustrative rather than a restrictive manner.

We Claim:

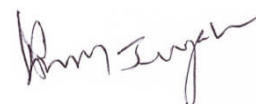
CLEAN COPY

1. A process for synthesizing clathrate hydrates in interstellar environment at low pressure of 10^{-10} mbar and at cryogenic temperatures in the range of 10 K to 135 K, the said process comprises;
 - 5 a. condensing the water vapour and guest molecule separately or together in a ultrahigh vacuum chamber and
 - b. gradually annealing the condensed mixture obtained from step (a) to temperatures below the desorption temperature of the guest molecule in vacuum for 0-48 hours wherein, the gradual prolonged annealing of the condensed guest molecule and water vapour mixture to temperatures below the desorption temperature of the guest molecule enhances the molecular mobility and H-bonding interaction for the entrapment of molecule in in-situ, forming clathrate hydrate cages.
- 10 2. The process as claimed in claim 1, wherein the guest molecule includes methane, carbon dioxide, acetone and tetrahydrofuran (THF).
- 15 3. The process as claimed in claim 1, wherein clathrate hydrates includes methane hydrate, carbon dioxide hydrate, acetone hydrate, and tetrahydrofuran hydrate.
4. The process as claimed in claim 3, wherein methane hydrate is formed by gradual annealing of CH_4 and water vapour mixture to 30 K for 25 hours.
5. The process as claimed in claim 3, wherein carbon dioxide hydrate is formed by keeping
20 of CO_2 and water vapour mixture to 10 K for 48 hours.
6. The process as claimed in claim 3, wherein acetone hydrate is formed by gradual annealing of acetone and water vapour mixture to 135 K.
7. The process as claimed in claim 3, wherein tetrahydrofuran hydrate is formed by gradual annealing of THF and water vapour mixture to 130 K for 6 hours.
- 25 8. The process as claimed in claim 6, wherein acetone hydrate transforms into cubic crystalline ice upon in-situ dissociation at 130-135 K over 3 hours.

Dated at Chennai this January 07, 2021

30

Signature:



D. Moses Jeyakaran
Advocate & Patent Agent
IN/PA — 369

A PROCESS FOR LOW TEMPERATURE, LOW PRESSURE SYNTHESIS OF CLATHRATE HYDRATES

5

ABSTRACT

The present invention relates to a process for synthesizing clathrate hydrates in ultrahigh vacuum at low pressure of 10^{-10} mbar and at temperatures in the range of 10 K to 135 K. Specifically the present invention relates to formation of methane, carbon dioxide, acetone, and tetrahydrofuran hydrates in extreme low-pressure environments. High molecular mobility and H-bonding play important roles in the entrapment of guest molecules in the in-situ formation of clathrate hydrates cages. This finding implies that CHs can exist in extreme low-pressure environments present in the ISM. These hydrates in ISM, subjected to various chemical processes that act as sources for relevant prebiotic molecules.

10

15

Application Number: 201841049836

5 A PROCESS FOR LOW TEMPERATURE, LOW PRESSURE SYNTHESIS OF CLATHRATE HYDRATES

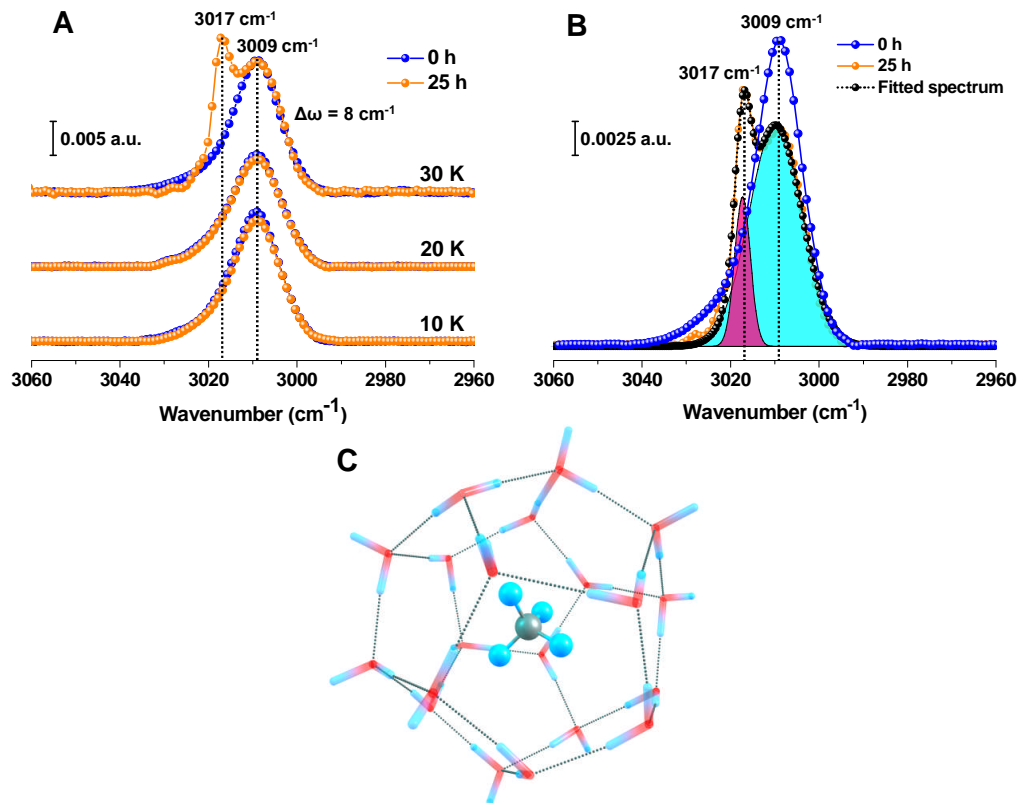
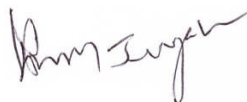


FIGURE 1

Signature: 

D. Moses Jeyakaran
Advocate & Patent Agent
IN/PA — 369

Application Number: 201841049836

5 A PROCESS FOR LOW TEMPERATURE, LOW PRESSURE SYNTHESIS OF CLATHRATE HYDRATES

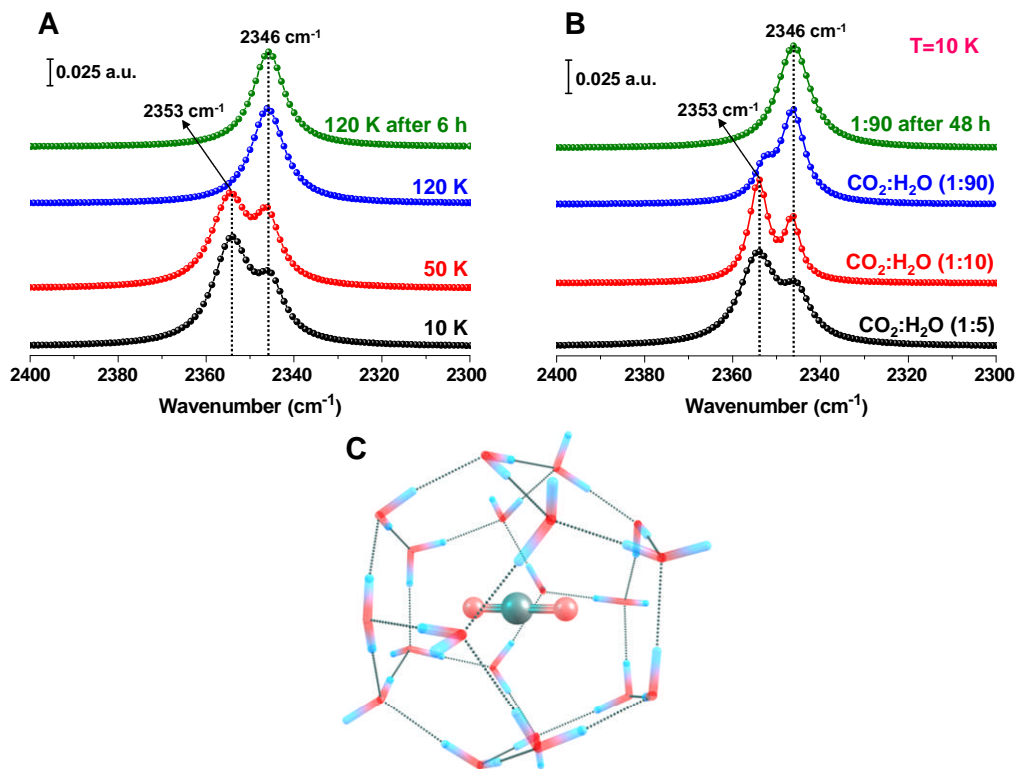


FIGURE 2

Signature: *[Handwritten Signature]*

D. Moses Jeyakaran
Advocate & Patent Agent
IN/PA — 369

Application Number: 201841049836

5 A PROCESS FOR LOW TEMPERATURE, LOW PRESSURE SYNTHESIS OF CLATHRATE HYDRATES

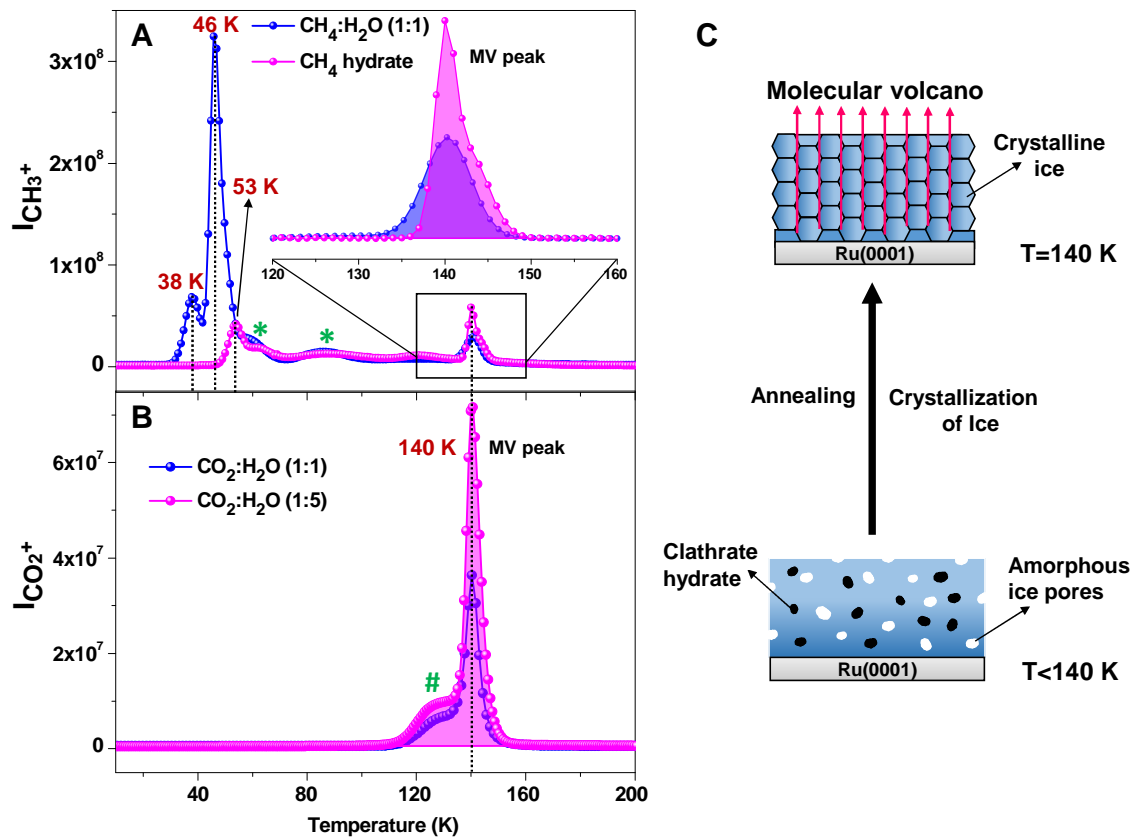


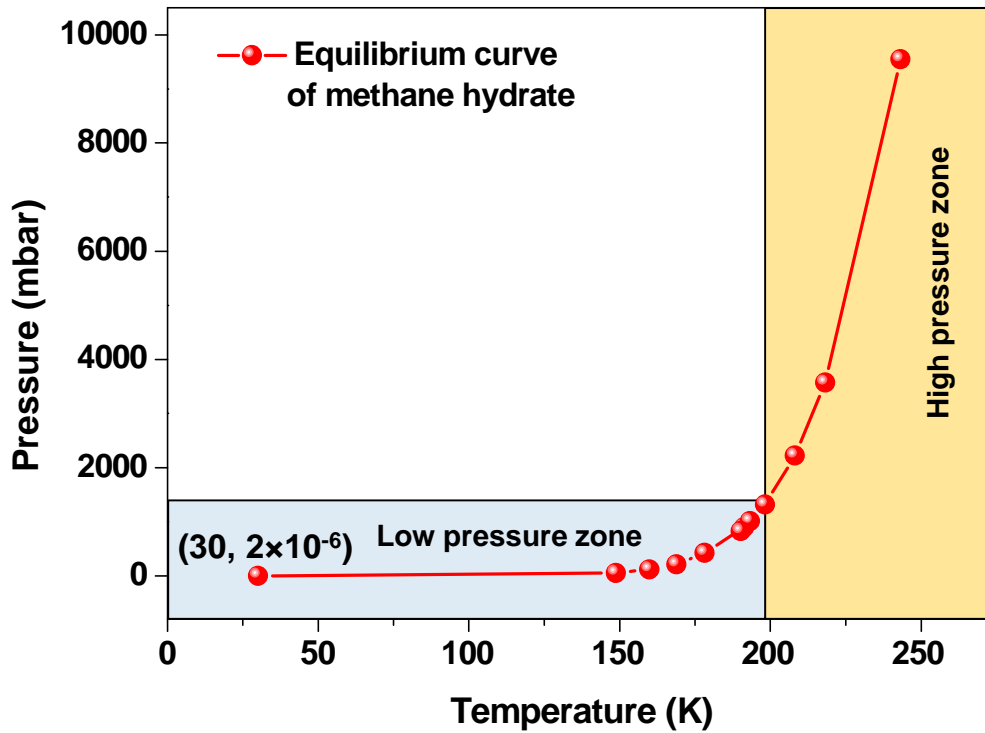
FIGURE 3

Signature:

D. Moses Jeyakaran
Advocate & Patent Agent
IN/PA — 369

Application Number: 201841049836

5 A PROCESS FOR LOW TEMPERATURE, LOW PRESSURE SYNTHESIS OF CLATHRATE HYDRATES



10

FIGURE 4

15

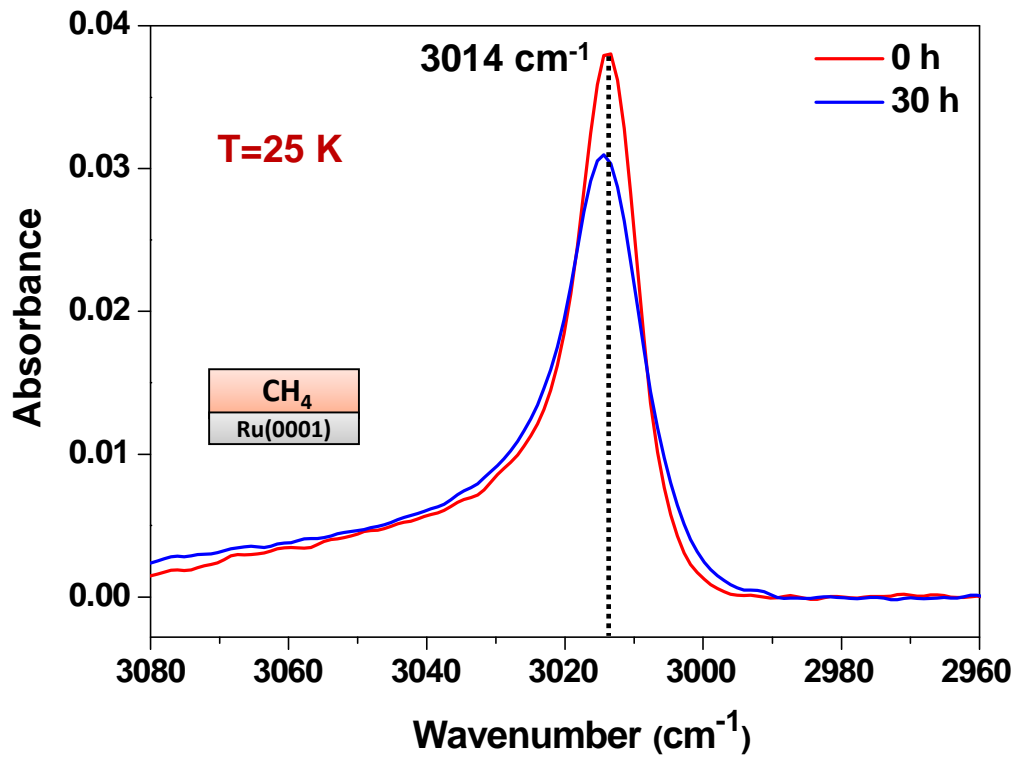
Signature: 

D. Moses Jeyakaran
Advocate & Patent Agent
IN/PA — 369

20

Application Number: 201841049836

5 A PROCESS FOR LOW TEMPERATURE, LOW PRESSURE SYNTHESIS OF CLATHRATE HYDRATES



10

FIGURE 5

15

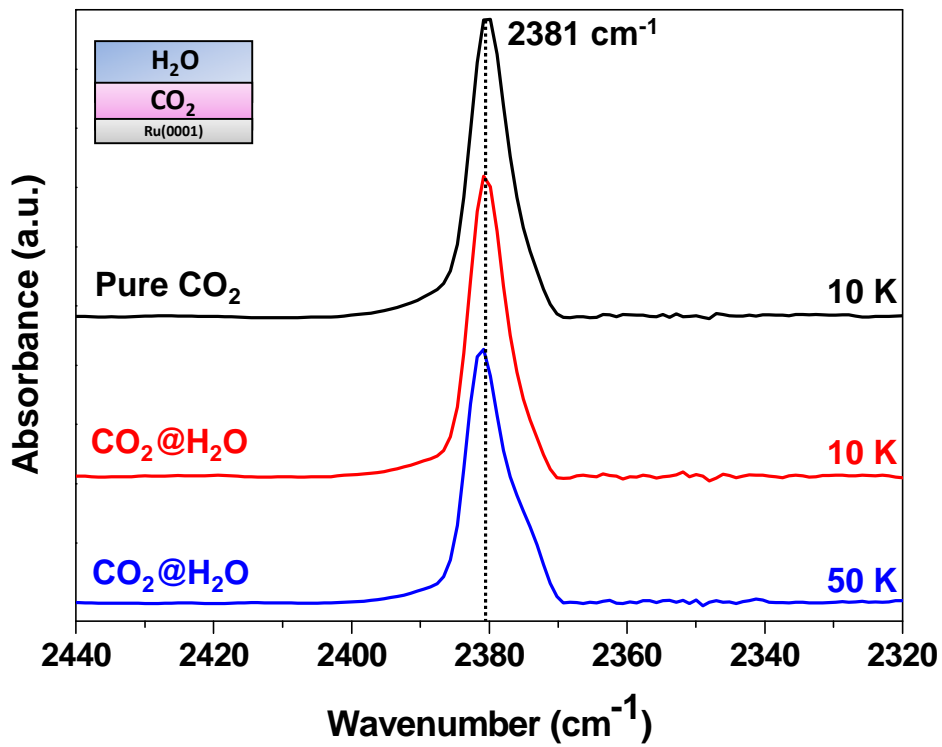
Signature:

D. Moses Jeyakaran
Advocate & Patent Agent
IN/PA — 369

20

Application Number: 201841049836

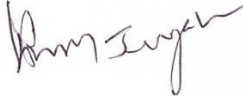
5 A PROCESS FOR LOW TEMPERATURE, LOW PRESSURE SYNTHESIS OF CLATHRATE HYDRATES



10

FIGURE 6

15

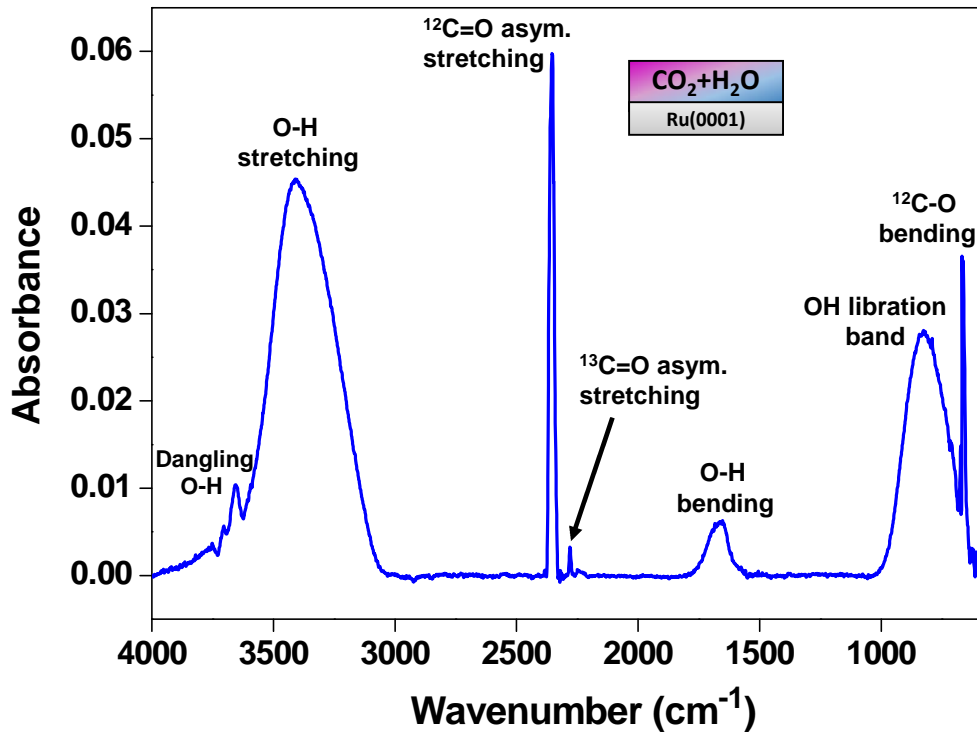
Signature: 

D. Moses Jeyakaran
Advocate & Patent Agent
IN/PA — 369

20

Application Number: 201841049836

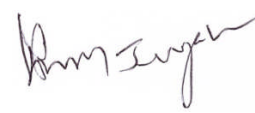
5 A PROCESS FOR LOW TEMPERATURE, LOW PRESSURE SYNTHESIS OF CLATHRATE HYDRATES



10

FIGURE 7

15

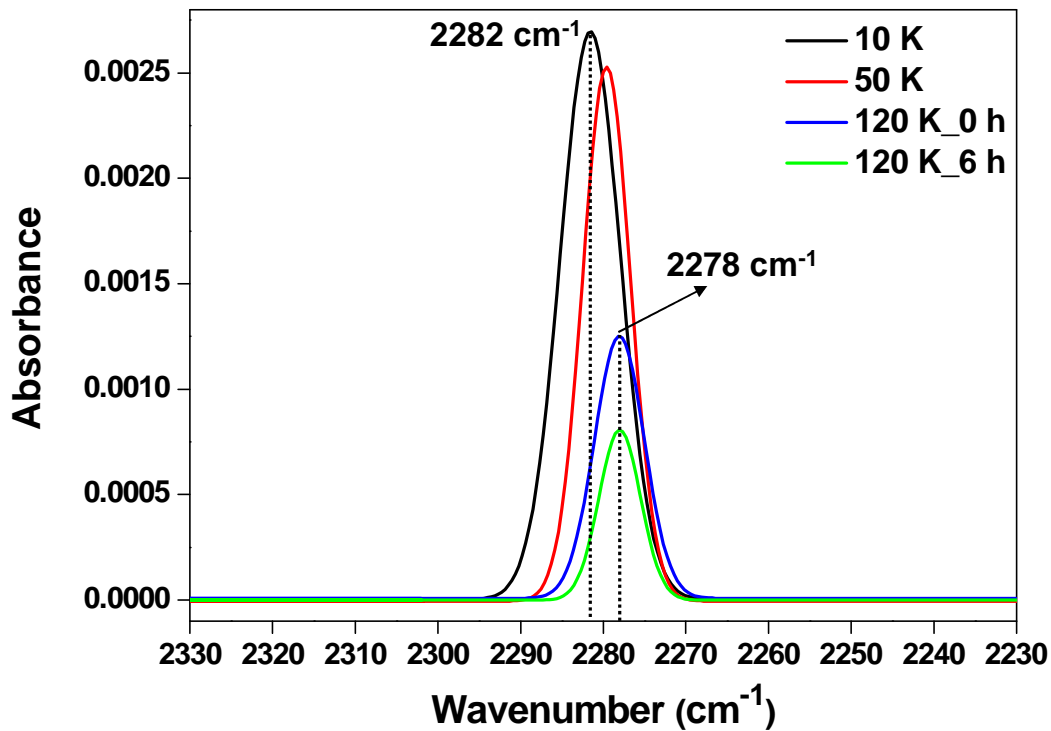
Signature: 

D. Moses Jeyakaran
Advocate & Patent Agent
IN/PA — 369

20

Application Number: 201841049836

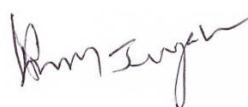
5 A PROCESS FOR LOW TEMPERATURE, LOW PRESSURE SYNTHESIS OF CLATHRATE HYDRATES



10

FIGURE 8

15

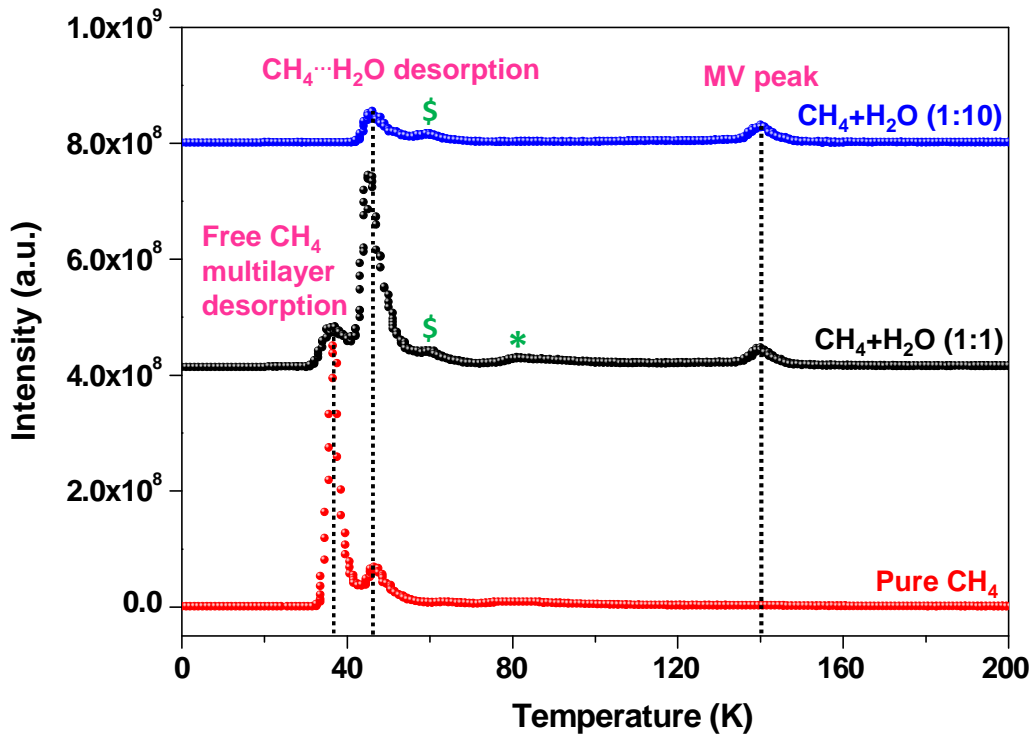
Signature: 

D. Moses Jeyakaran
Advocate & Patent Agent
IN/PA — 369

20

Application Number: 201841049836

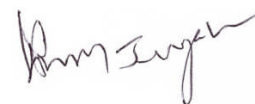
5 A PROCESS FOR LOW TEMPERATURE, LOW PRESSURE SYNTHESIS OF CLATHRATE HYDRATES



10

FIGURE 9

15

Signature: 

D. Moses Jeyakaran
Advocate & Patent Agent
IN/PA — 369

20

Application Number: 201841049836

5 A PROCESS FOR LOW TEMPERATURE, LOW PRESSURE SYNTHESIS OF CLATHRATE HYDRATES

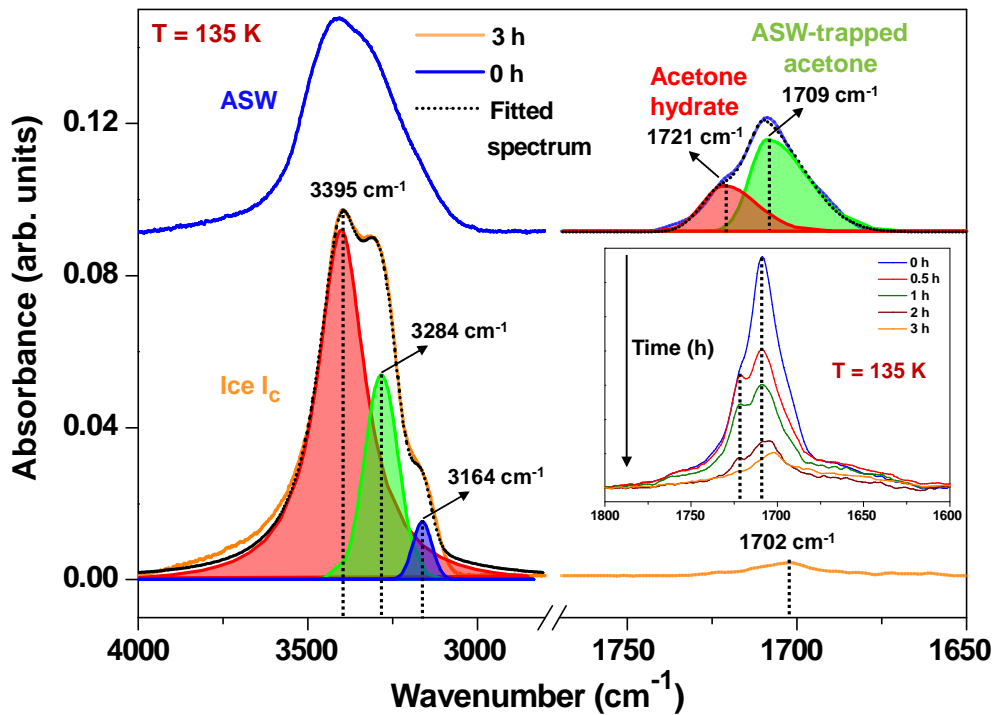
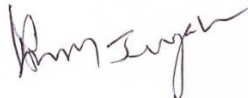


FIGURE 10

10

Signature: 

15

D. Moses Jeyakaran
Advocate & Patent Agent
IN/PA — 369

20

Application Number: 201841049836

5 A PROCESS FOR LOW TEMPERATURE, LOW PRESSURE SYNTHESIS OF CLATHRATE HYDRATES

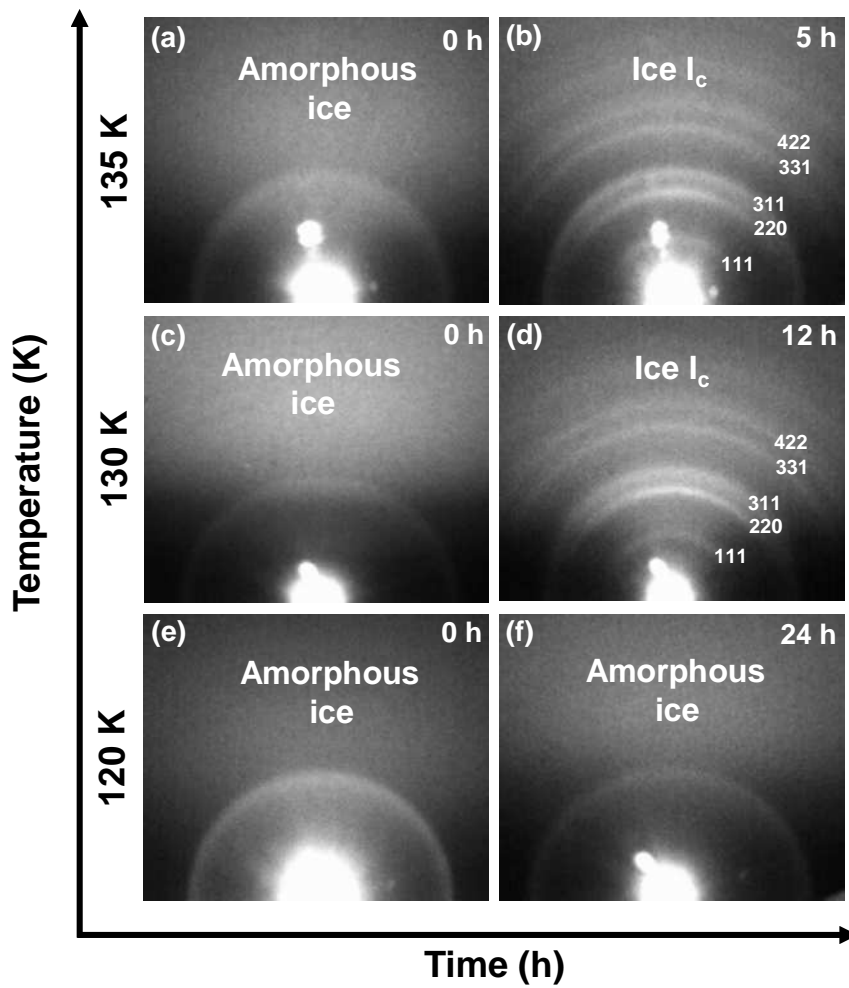
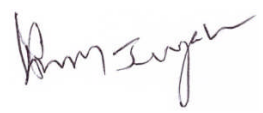


FIGURE 11

10

Signature: 

D. Moses Jeyakaran
Advocate & Patent Agent
IN/PA — 369

15

Application Number: 201841049836

5 A PROCESS FOR LOW TEMPERATURE, LOW PRESSURE SYNTHESIS OF CLATHRATE HYDRATES

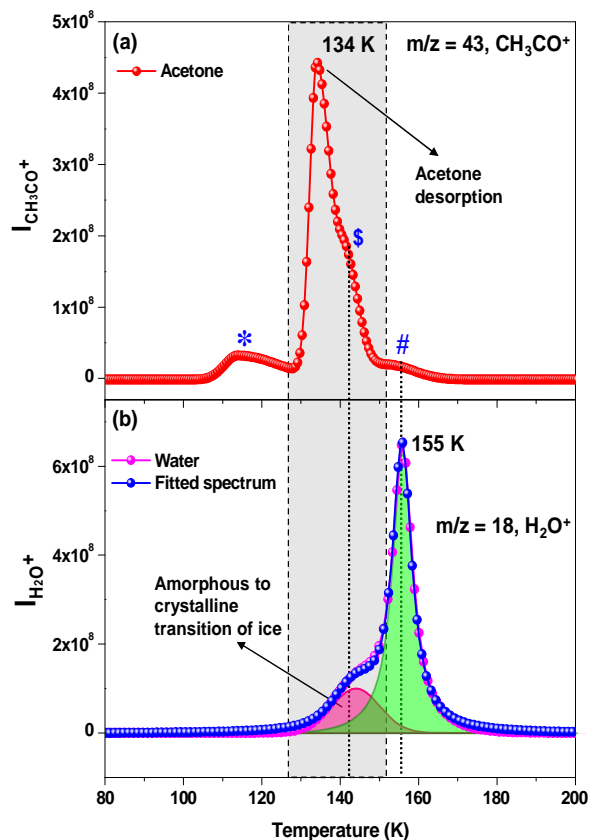
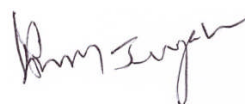


FIGURE 12

10

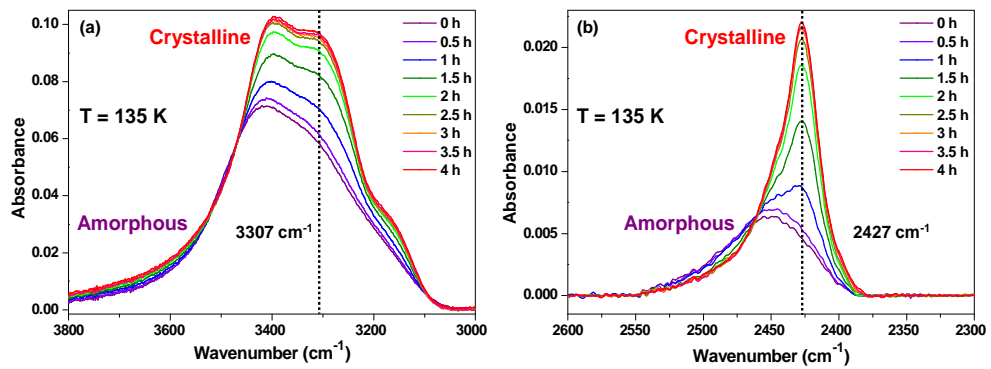
Signature: 

15

D. Moses Jeyakaran
 Advocate & Patent Agent
 IN/PA — 369

Application Number: 201841049836

5 A PROCESS FOR LOW TEMPERATURE, LOW PRESSURE SYNTHESIS OF CLATHRATE HYDRATES



10

FIGURE 13

15

Signature:

D. Moses Jeyakaran
Advocate & Patent Agent
IN/PA — 369

20

25

30

Application Number: 201841049836

5 A PROCESS FOR LOW TEMPERATURE, LOW PRESSURE SYNTHESIS OF CLATHRATE HYDRATES

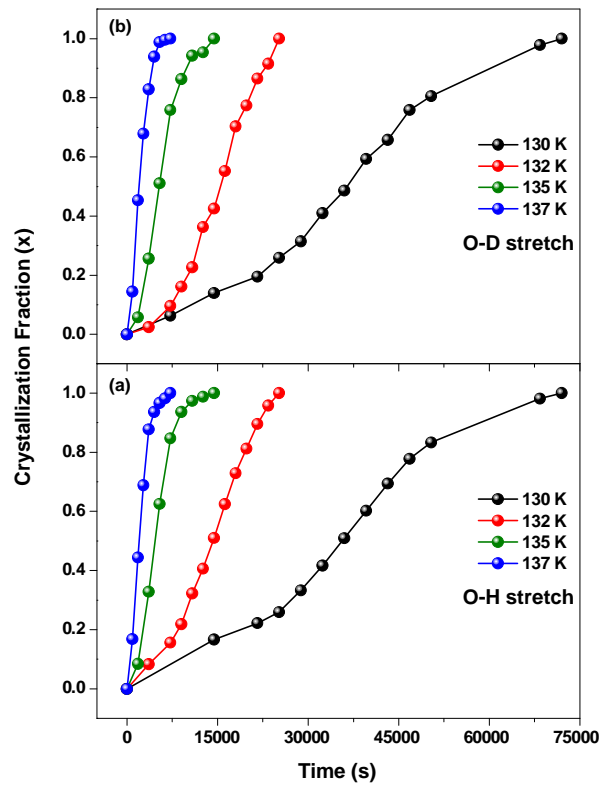
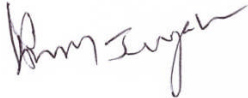


FIGURE 14

10

Signature: 

15

D. Moses Jeyakaran
Advocate & Patent Agent
IN/PA — 369

20

Application Number: 201841049836

5 A PROCESS FOR LOW TEMPERATURE, LOW PRESSURE SYNTHESIS OF CLATHRATE HYDRATES

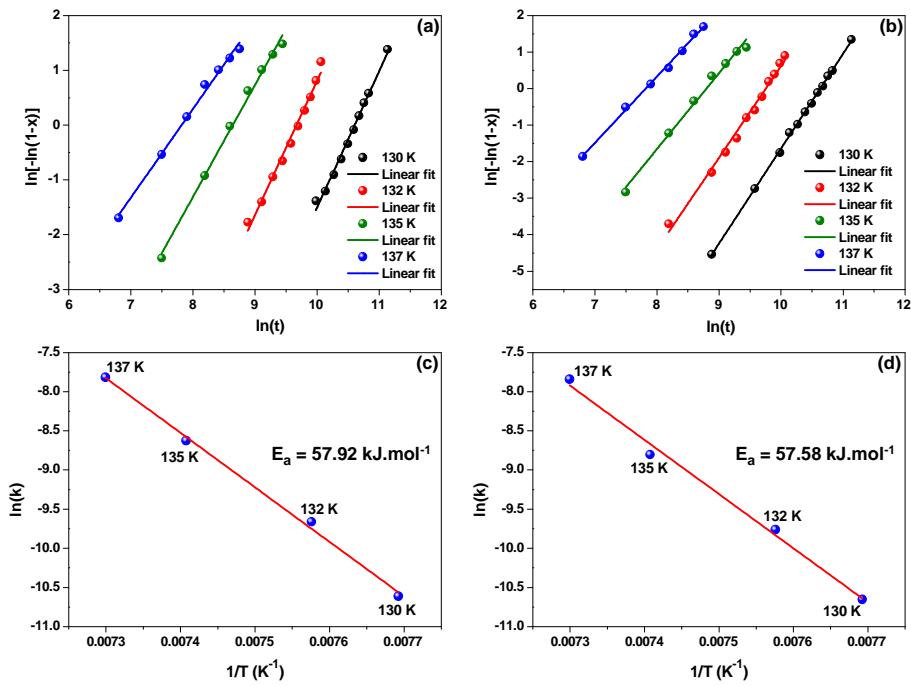
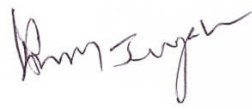


FIGURE 15

10

Signature: 

15

D. Moses Jeyakaran
Advocate & Patent Agent
IN/PA — 369

20

25

Application Number: 201841049836

A PROCESS FOR LOW TEMPERATURE, LOW PRESSURE SYNTHESIS OF CLATHRATE HYDRATES

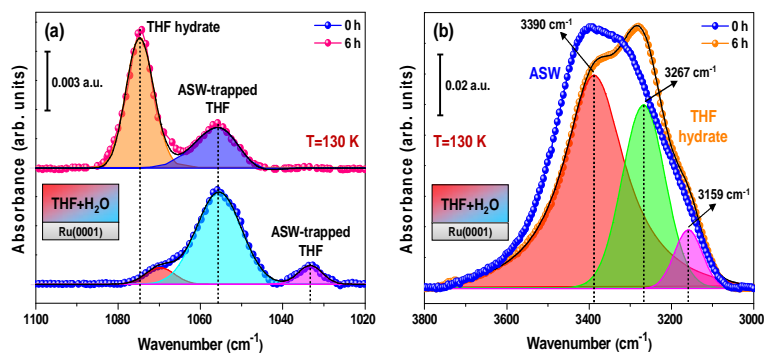


FIGURE 16

Signature:

D. Moses Jeyakaran
Advocate & Patent Agent
IN/PA — 369

Application Number: 201841049836

5 A PROCESS FOR LOW TEMPERATURE, LOW PRESSURE SYNTHESIS OF CLATHRATE HYDRATES

10

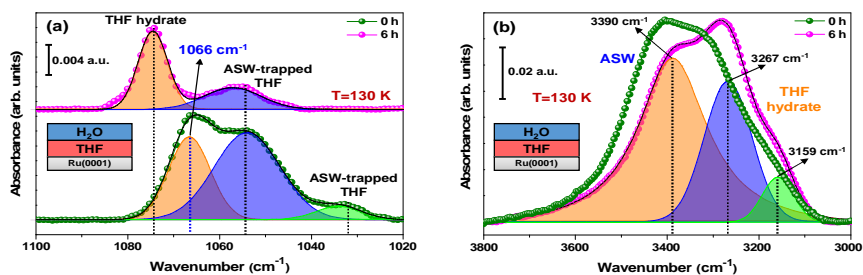


FIGURE 17

15

Signature: *D. Moses Jeyakaran*

D. Moses Jeyakaran
Advocate & Patent Agent
IN/PA — 369

20

25

30

35

Application Number: 201841049836

5 A PROCESS FOR LOW TEMPERATURE, LOW PRESSURE SYNTHESIS OF CLATHRATE HYDRATES

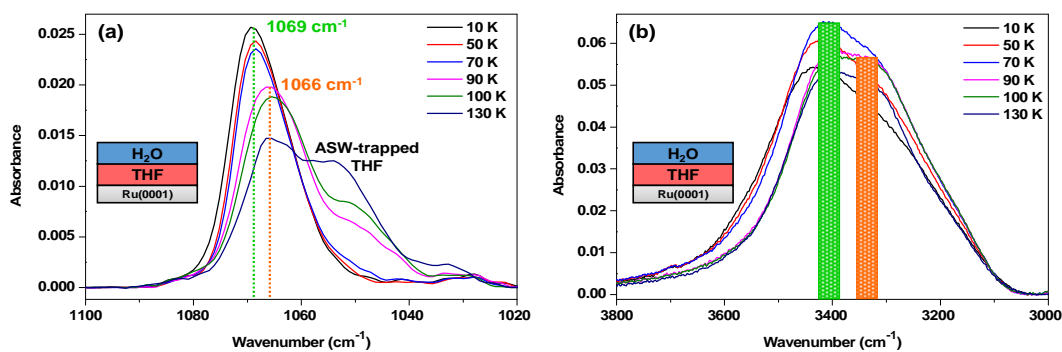


FIGURE 18

10

Signature: *D. Moses Jeyakaran*

15

D. Moses Jeyakaran
Advocate & Patent Agent
IN/PA — 369

20

25

30

Application Number: 201841049836

5 A PROCESS FOR LOW TEMPERATURE, LOW PRESSURE SYNTHESIS OF CLATHRATE HYDRATES

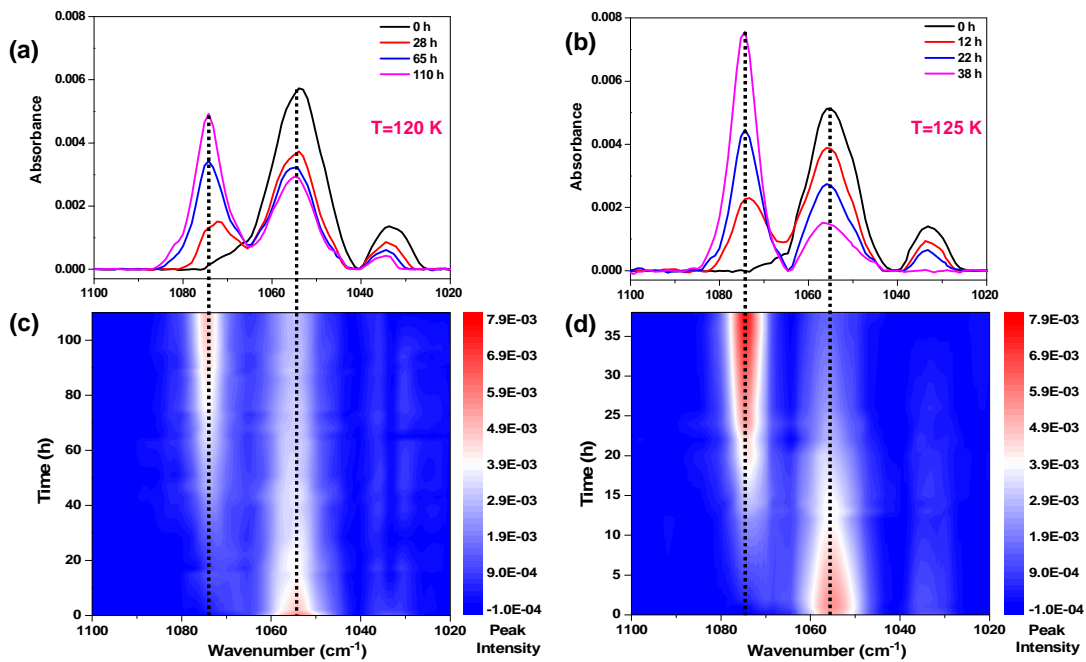
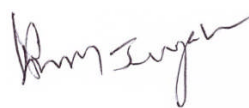


FIGURE 19

10

Signature: 

15

D. Moses Jeyakaran
Advocate & Patent Agent
IN/PA — 369

20

Application Number: 201841049836

5 A PROCESS FOR LOW TEMPERATURE, LOW PRESSURE SYNTHESIS OF CLATHRATE HYDRATES

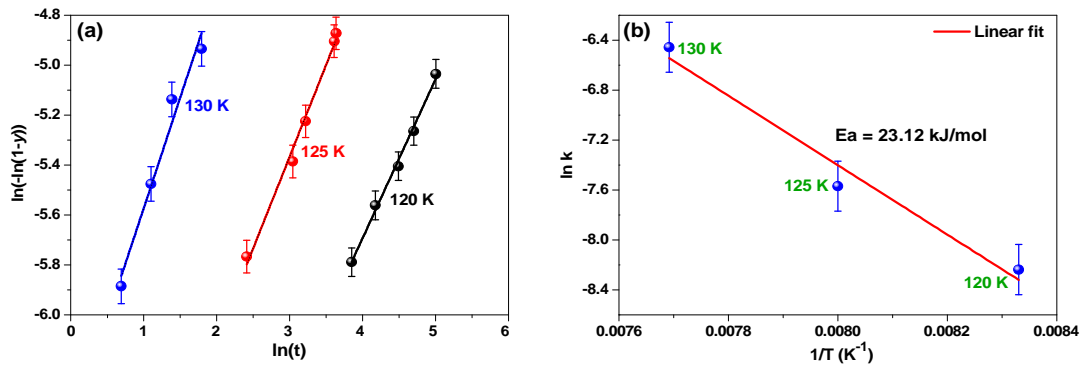


FIGURE 20

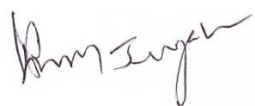
10

15

20

25

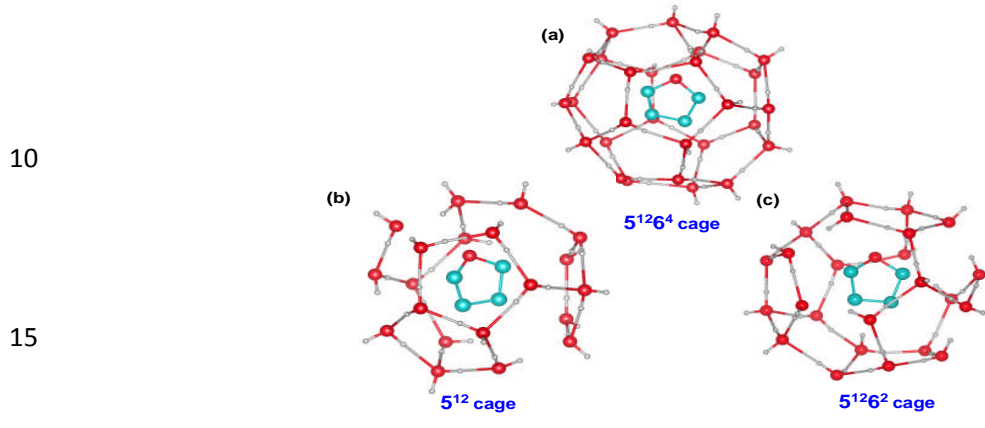
30

Signature: 

D. Moses Jeyakaran
Advocate & Patent Agent
IN/PA — 369

Application Number: 201841049836

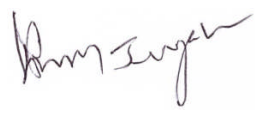
5 A PROCESS FOR LOW TEMPERATURE, LOW PRESSURE SYNTHESIS OF CLATHRATE HYDRATES



20

FIGURE 21

25

Signature: 

D. Moses Jeyakaran
Advocate & Patent Agent
IN/PA — 369

30